

Response to Comments of Editor

(Comments in *italics*)

Manuscript number: acp-2021-119

Title: Impacts of aerosol-photolysis interaction and aerosol-radiation feedback on surface-layer ozone in North China during a multi-pollutant air pollution episode

The reviewer makes some constructive suggestions which are generally in line with my earlier comments. The paper has improved from the earliest submissions, and I think that it can still improve with attention to these comments.

Response:

Additional simulations have been conducted following the Reviewer's comments, and the results from these new simulations also support the general conclusion we obtained in the manuscript.

As described below in our point-to-point responses, we have carefully revised the manuscript and addressed the Reviewer's comments.

Response to Comments of Reviewer #2

(Comments in *italics*)

Manuscript number: acp-2021-119

Title: Impacts of aerosol-photolysis interaction and aerosol-radiation feedback on surface-layer ozone in North China during a multi-pollutant air pollution episode

This revised paper is well written and well reasoned but in previous round of review, several key issues were pointed out. Specifically in the last round of review, the editor posed three key questions that the authors needed to address in the manuscript with which I agree.

1) What is the goal of the paper - to consider high air pollution conditions, and for what purpose?

2) Why were the episodes chosen, and what do we hope to learn more generally for other conditions?

3) How do the conclusions based on the CAPA episodes relate with other conditions during the years studied (2014-16) and to what extent are they relevant for other years before or after?

I believe that the authors have fully answered question 1 and the clear motivation has improved the manuscript. However, the current revision only partially answers questions 2 and 3. My major and minor comments are as follows:

Response:

Thanks to the Reviewer for the valuable comments and suggestions which are helpful for improving our manuscript. We have revised the manuscript carefully, as described in our point-to-point responses to the comments.

Major Comments:

1a) The authors addressed the questions about other conditions by conducting 3 additional simulations with conditions other than complex air pollution episodes. These simulations are important and reveal some interesting findings. Particularly, the O₃ decrease in a high PM episode from API and ARF is close to double the impact in a complex episode and in cases without high PM pollution the impact is close to half the impact of a complex episode. However, the authors treat these cases as an afterthought with them being mentioned only in the last few lines of the conclusion/supplementary material. These cases need to be incorporated into the main text as another results section and they need more descriptive names such as: High PM_{2.5} (HI_PM), Low Pollution (LOW_POL), and High O₃ (HI_O₃).

Response:

The main purpose of this study is to quantify the respective/combined impacts of ARF and API on surface O₃ concentrations during complex air pollution episodes, as

stated in the title of the manuscript. We thank the Reviewer for the positive comment on the motivation of this study.

In order to make the conclusions more general, another six simulations under different air pollution conditions (i.e., PM_{2.5} pollution alone, O₃ pollution alone, and neither PM_{2.5} nor O₃ exceed air quality standard), as suggested by the Editor and the Reviewer, are conducted. All the results confirm the same conclusion that the reduction in O₃ by API is larger than that by ARF.

In the revised manuscript, we have changed the names of these additional simulations following the suggestion of the Reviewer. In order not to distract from the major purpose of the article, we have added a new section of ‘Discussions’ before the Conclusions to present the results from these additional simulations.

“We presented above the results from our simulations of multi-pollutant air pollution episodes. In order to make the conclusion be more general, we carried out simulations for three additional air pollution conditions, i.e., (1) PM_{2.5} pollution alone (High_PM, with daily mean PM_{2.5} concentration larger than 75 $\mu\text{g m}^{-3}$), (2) O₃ pollution alone (High_O₃, with the maximum daily 8-h average O₃ concentration larger than 80 ppb), and (3) neither PM_{2.5} nor O₃ exceeded air quality standard (Low_POL, with daily mean PM_{2.5} and the maximum daily 8-h average O₃ concentrations smaller than 75 $\mu\text{g m}^{-3}$ and 80 ppb, respectively). For each condition of air pollution, we examined two episodes.

Figures S12 and S13 show the temporal variations of observed and simulated PM_{2.5} and O₃ concentrations during 7-12 October 2014 (High_PM_Episode1), 7-11 April 2014 (High_PM_Episode2), 15-21 June 2017 (High_O₃_Episode1), 12-17 July 2017 (High_O₃_Episode2), 13-18 June 2016 (Low_POL_Episode1), and 13-17 July 2016 (Low_POL_Episode2). The temporal variations of observed PM_{2.5} can be well captured by the model with IOAs of 0.63, 0.82, 0.56, 0.42, 0.76 and 0.54, and NMBs of 7.4%, 20.3%, -21.7%, -25.9%, 14.7% and -29.3% during High_PM_Episode1, High_PM_Episode2, High_O₃_Episode1, High_O₃_Episode2, Low_POL_Episode1, and Low_POL_Episode2, respectively. The model also simulates well the diurnal variation of O₃ over the North China, with IOAs of 0.87, 0.80, 0.87, 0.90, 0.84 and 0.86, and NMBs of -9.4%, -29.5%, -15.2%, -9.4%, 11.6% and 18.0% in these six episodes, respectively.

Figure 9 shows changes in daytime surface-layer O₃ due to API, ARF, and the combined effects (denoted as ALL) of High_PM_Episode1, High_PM_Episode2, High_O₃_Episode1, High_O₃_Episode2, Low_POL_Episode1, and Low_POL_Episode2. As summarized in Table 2, all the simulations confirm the same conclusion that the reduction in O₃ by API is larger than that by ARF. Averaged over the entire domain, the percentage reductions in O₃ by API and ARF are, respectively, 29.3% and 6.2% in High_PM_Episode1, 16.9% and 4.7% in High_PM_Episode2, 5.3% and 0.1% in High_O₃_Episode1, 4.5% and 0.1% in High_O₃_Episode2, 6.8% and 1.0% in Low_POL_Episode1, and 2.9% and 0.7% in Low_POL_Episode2. It’s worth noting that the percentage reductions in O₃ from both API and ARF in High_PM episodes are 1.6~3.2 times the impacts in the complex episodes, while the impacts in cases of Low_POL and High_O₃ are 0.3~0.7 times the impacts of complex episodes.”

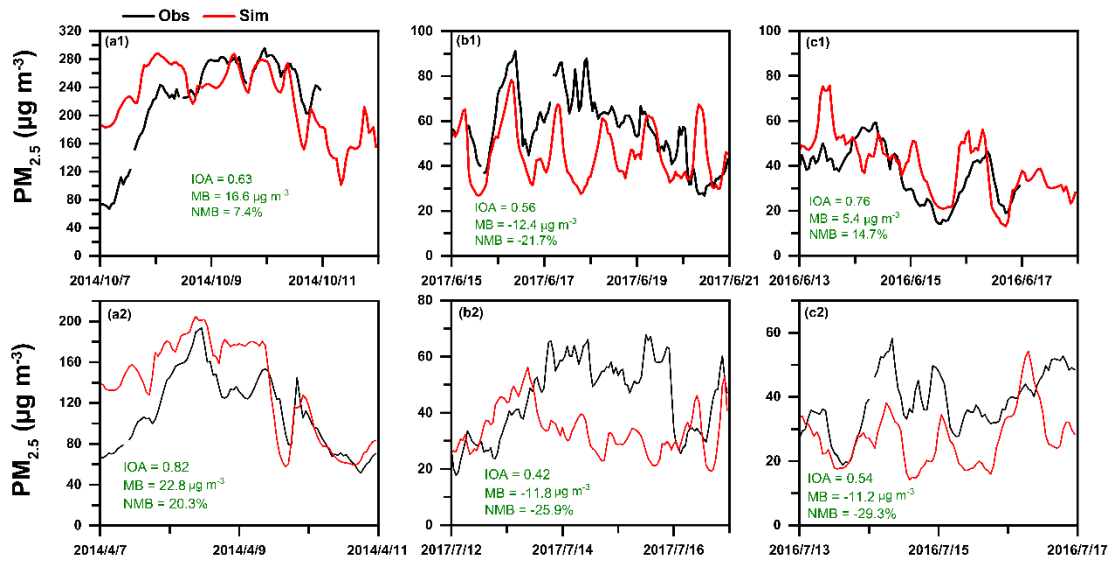


Figure S12. Time series of observed (black) and simulated (red) hourly surface-layer PM_{2.5} concentrations averaged over the thirty-two observation sites in Beijing, Tianjin, and Baoding during 7-12 October 2014 (High_PM_Episode1), 7-11 April 2014 (High_PM_Episode2), 15-21 June 2017 (High_O₃_Episode1), 12-17 July 2017 (High_O₃_Episode2), 13-18 June 2016 (Low_POL_Episode1), and 13-17 July 2016 (Low_POL_Episode2). The index of agreement (IOA), mean bias (MB), and normalized mean bias (NMB) are also shown.

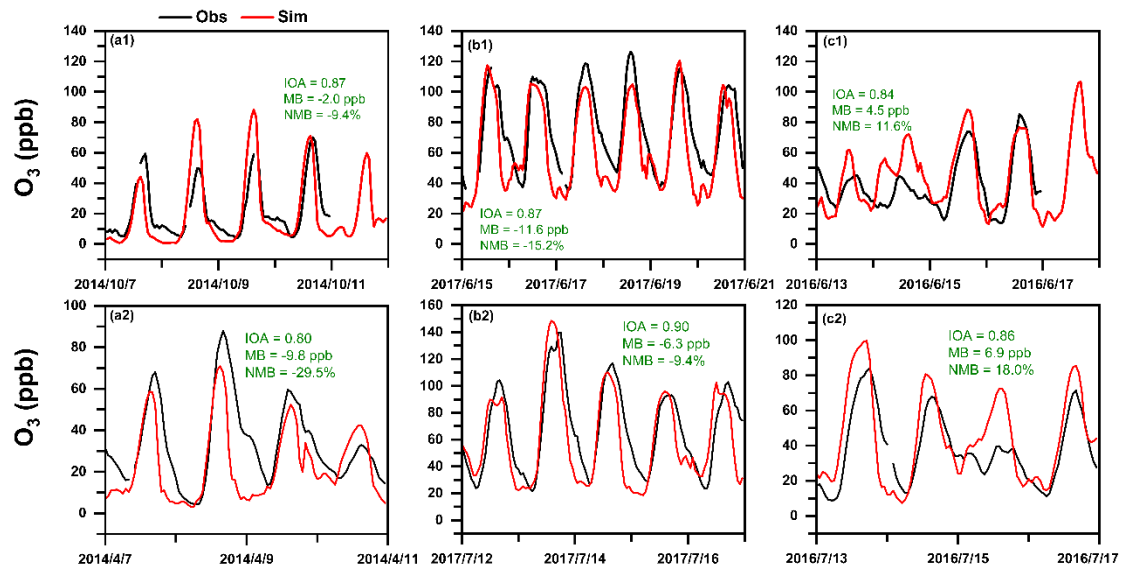


Figure S13. The same as Fig. S12, but for O₃.

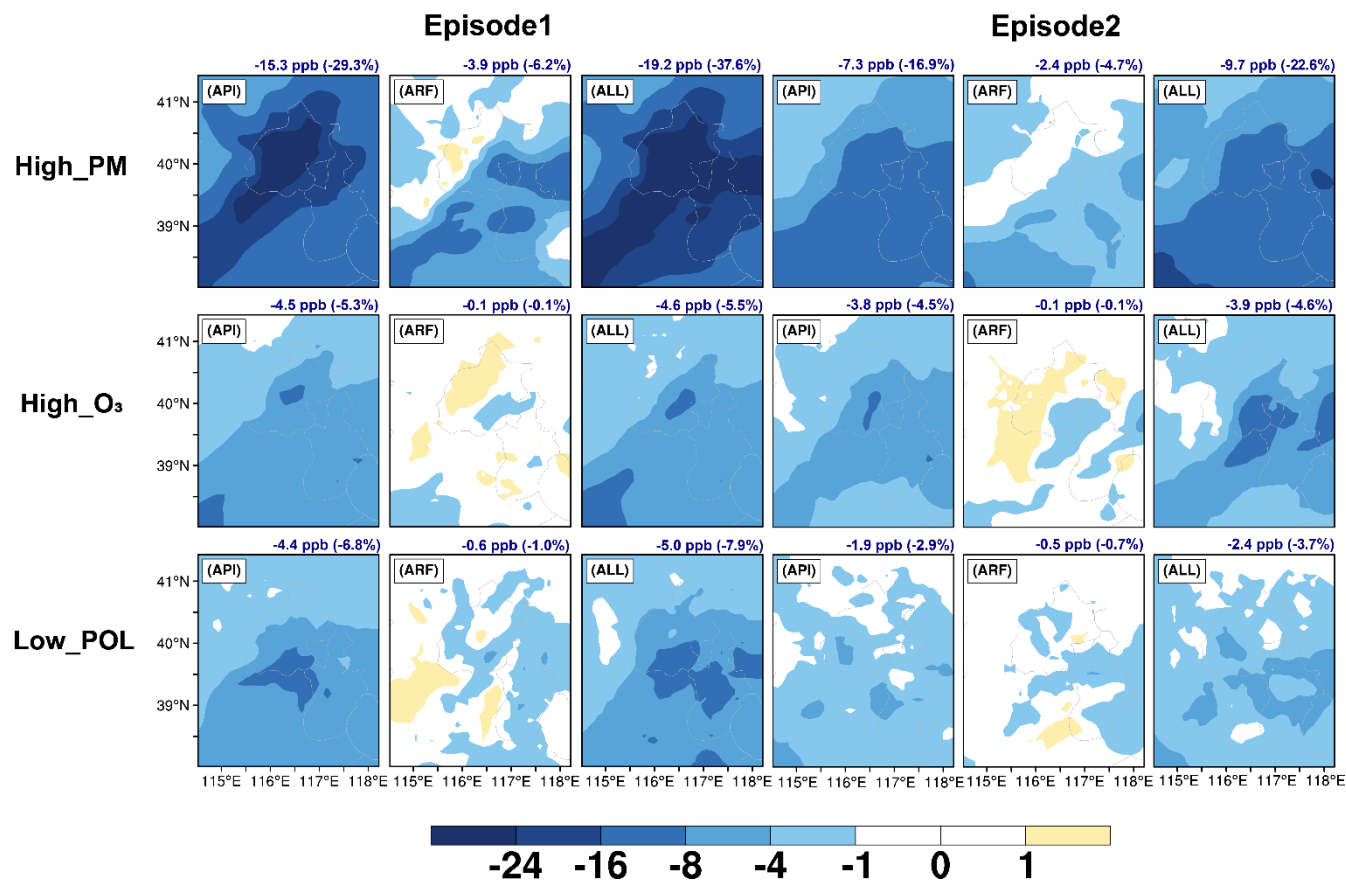


Figure 9. The changes in surface-layer O₃ due to aerosol-photolysis interaction (API), aerosol-radiation feedback (ARF), and the combined effects (ALL, API+ARF) in the daytime (08:00-17:00 LST) of 7-12 October 2014 (High_PM_Episode1), 7-11 April 2014 (High_PM_Episode2), 15-21 June 2017 (High_O₃_Episode1), 12-17 July 2017 (High_O₃_Episode2), 13-18 June 2016 (Low_POL_Episode1), and 13-17 July 2016 (Low_POL_Episode2). The changes (percentage changes) in O₃ concentrations caused by API, ARF and ALL averaged over the entire simulated domain are also shown at the top of each panel.

Table 2. Detailed information of the analyzed episodes, including the impacts of API, ARF and ALL on O₃ concentrations under different air pollution conditions. The numbers in bold indicate the concentrations exceeded the Class II limit of the National Ambient Air Quality Standards of China. The numbers in parentheses indicate the percentage changes in O₃ concentration.

Type	Episode	Time	PM _{2.5} pollution ($\mu\text{g m}^{-3}$)	O ₃ pollution (ppb)	API (ppb)	ARF (ppb)	ALL (ppb)
Complex air pollution	Episode1	2014.7.28-2014.8.3	113.3	80.0	-8.5 (-10.2%)	-2.9 (-3.2%)	-11.4 (-13.7%)
	Episode2	2015.7.8-2015.7.13	79.3	89.6	-10.3 (-11.8%)	-1.0 (-1.1%)	-11.3 (-13.0%)
	Episode3	2016.6.5-2016.6.11	76.5	87.6	-9.1 (-11.2%)	-0.9 (-1.0%)	-10.0 (-12.3%)
	Episode4	2017.6.28-2017.7.3	75.4	113.8	-11.4 (-12.2%)	0.7 (0.5%)	-10.7 (-11.6%)
High_PM	Episode1	2014.10.7-2014.10.12	223.5	46.9	-15.3 (-29.3%)	-3.9 (-6.2%)	-19.2 (-37.6%)
	Episode2	2014.4.7-2014.4.11	111.7	54.8	-7.3 (-16.9%)	-2.4 (-4.7%)	-9.7 (-22.6%)
High_O₃	Episode1	2017.6.15-2017.6.21	61.9	103.6	-4.5 (-5.3%)	-0.1 (-0.1%)	-4.6 (-5.5%)
	Episode2	2017.7.12-2017.7.17	45.6	100.4	-3.8 (-4.5%)	-0.1 (-0.1%)	-3.9 (-4.6%)
Low_POL	Episode1	2016.6.13-2016.6.18	36.5	62.4	-4.4 (-6.8%)	-0.6 (-1.0%)	-5.0 (-7.9%)
	Episode2	2016.7.13-2016.7.17	38.3	55.9	-1.9 (-2.9%)	-0.5 (-0.7%)	-2.4 (-3.7%)

1b) *The authors should also consider possibly simulating an additional case with each of these conditions to see if the differences between them and the CAPAs are robust, or alternatively they should demonstrate that the episodes they selected are representative of those conditions throughout the period of interest (2014-2017).*

Response:

Following the Reviewer's suggestion, we have carried out simulation of one more case for each of air pollution conditions (i.e., High_PM_Episode2, High_O₃_Episode2, and Low_POL_Episode2). Please see our responses to your major comment 1a) for the results from these new simulations. All the results confirm the same conclusion that the reduction in O₃ by API is larger than that by ARF (Table 2).

2) *The authors have still not addressed historical conditions before 2014. The authors have stated this is because national observations are not available to pin-point complex air pollution episodes before 2013. However, the authors have also stated "Air pollution in China was characterized by high concentrations of PM_{2.5} before 2014 (Li et al., 2019a; Zhang et al., 2019) and by synchronous occurrence of high PM_{2.5} and O₃ or high levels of O₃ alone after 2017 (Dai et al., 2021; Li et al., 2019b; Li et al., 2020; Qin et al., 2021)." If there are no observations before 2013 to justify this statement, how is this statement supported? At a minimum, the authors should point out the lack of data before their period of interest in the manuscript as a reason they cannot explore the magnitudes of API and ARF before 2014. However, if the authors are at least aware of a high PM_{2.5} case from the 2001-2005 period it would be worth comparing that with the current HI_PM case to see if the magnitude of the API and ARF impacts have decreased in a significant way.*

Response to "If there are no observations before 2013 to justify this statement, how is this statement supported?"

The open official national data are not available before 2013 as the China National Environmental Monitoring Center (CNEMC) network was established in 2013 (Chinese State Council, 2013). Before 2013, only the US Embassy had publicly accessible and continuous PM_{2.5} observation data in Beijing. Daily PM_{2.5} from the US Embassy in Beijing is available between 18 February 2009 and 30 June 2017 (<http://www.stateair.net/web/historical/1/1.html>) and is shown in Fig. R1 below. PM_{2.5} concentrations were very high before 2014 (from 18 February 2009 to 31 December 2013), with 935 days (54%) above 75 µg m⁻³ and 345 days (20%) above 150 µg m⁻³ in Beijing, respectively. However, there were no observations of O₃ from the US Embassy, which make it difficult to select the time and location of complex air pollution events and to evaluate the model results before 2013.

The general situation of air pollution from 2013 to 2019 was presented by Li et al. (2020). As shown in Fig. R2 (see below, taken from Li et al. (2020)), since the implementation of the Chinese governmental Air Pollution Action Plan in 2013, the concentrations of PM_{2.5} decreased significantly, whereas the concentrations of O₃ increased steadily. Meanwhile, few episodes of complex air pollution events were

detected in north China in 2013 due to the high concentrations of $\text{PM}_{2.5}$ and low concentrations of O_3 . The observed annual mean concentrations of $\text{PM}_{2.5}$ decreased from $82.0 \mu\text{g m}^{-3}$ in 2014 to $49.8 \mu\text{g m}^{-3}$ in 2018 over the North China Plain (NCP) (Chen et al., 2020), which still exceeded the National Ambient Air Quality Standards ($35 \mu\text{g m}^{-3}$). Meanwhile, the summertime mean MDA8 O_3 concentrations frequently reached or exceeded the 80 ppb in NCP after 2017 (Fig. R2). That's why we say "Air pollution in China was characterized by high concentrations of $\text{PM}_{2.5}$ before 2014, and by synchronous occurrence of high $\text{PM}_{2.5}$ and O_3 or high levels of O_3 alone after 2017".

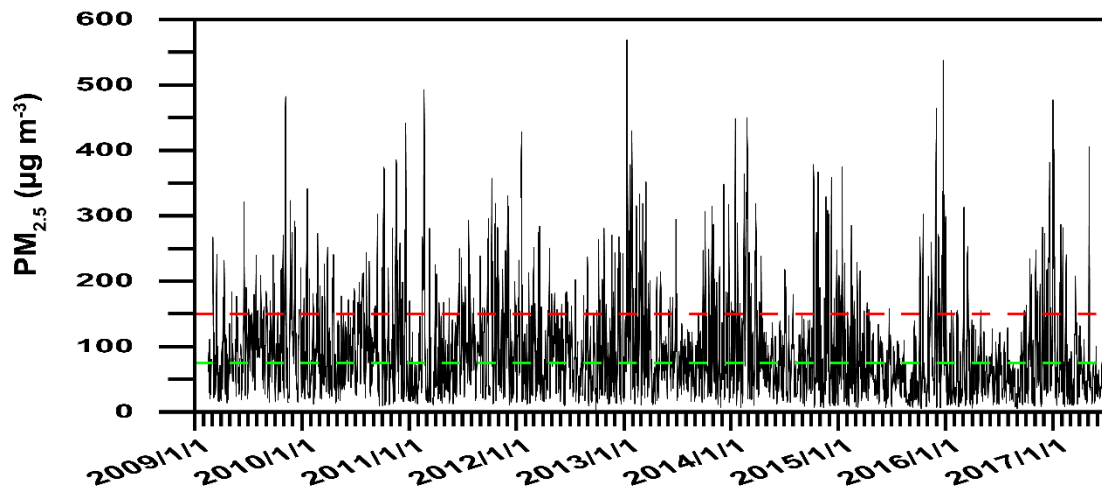


Figure R1. Time series of the observed daily $\text{PM}_{2.5}$ concentrations in Beijing from the US Embassy from 18 February 2009 to 30 June 2017. The green and red dash lines represent the concentrations of 75 and $150 \mu\text{g m}^{-3}$, respectively.

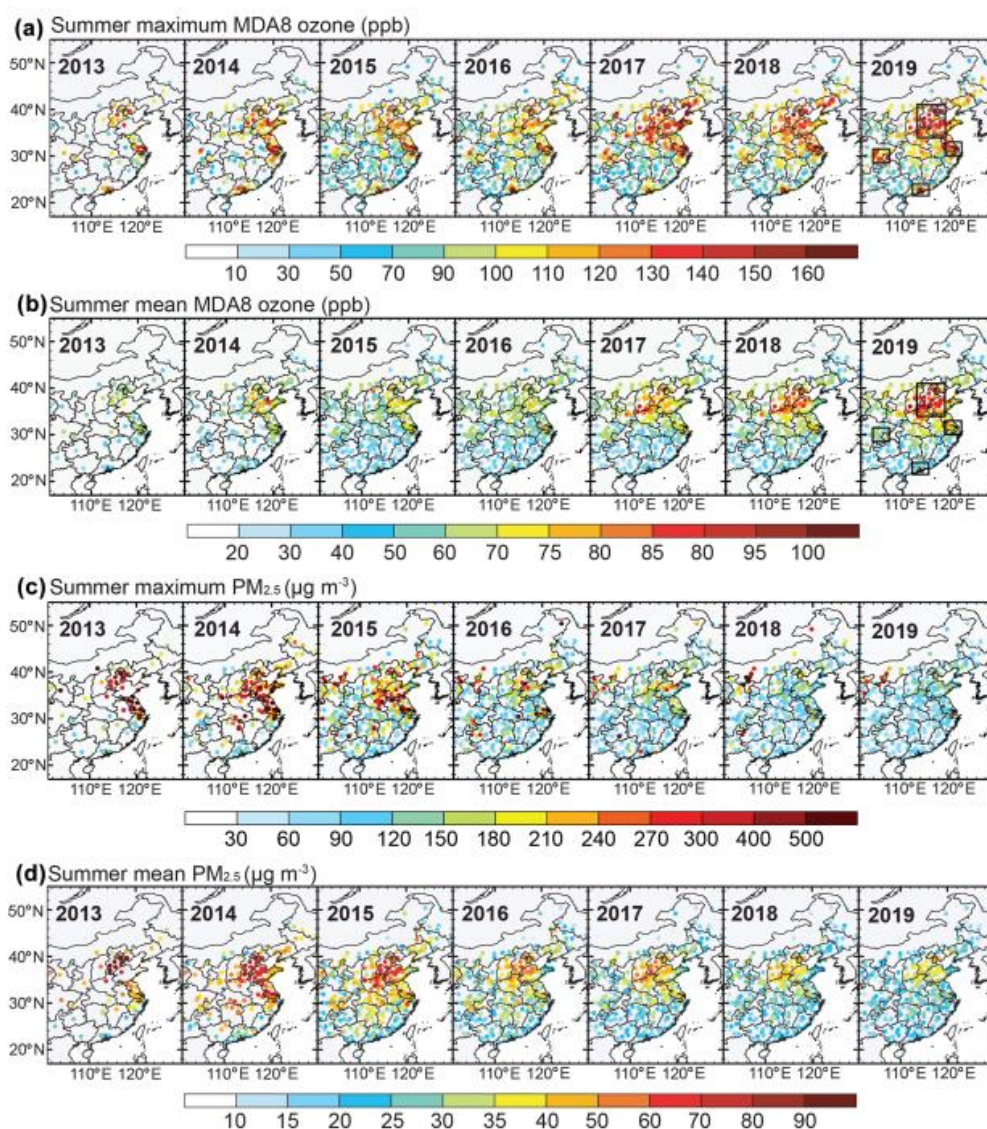


Figure R2. Summer (June-July-August) concentrations of maximum MDA8 ozone (a), mean MDA8 ozone (b), maximum PM_{2.5} (c), and mean PM_{2.5} (d) for 2013–2019 at the network operated by the China Ministry of Ecology and Environment (MEE). Rectangles denote the four megacity clusters: the North China Plain (NCP; 34–41 °N, 113–119 °E), the Yangtze River Delta (YRD; 30–33 °N, 119–122 °E), the Pearl River Delta (PRD; 21.5–24 °N, 112–115.5 °E), and the Sichuan Basin (SCB; 28.5–31.5 °N, 103.5–107 °E). (Li et al., 2020)

Response to “*At a minimum, the authors should point out the lack of data before their period of interest in the manuscript as a reason they cannot explore the magnitudes of API and ARF before 2014.*”

According to the Reviewer’s comments, the limitation section is updated in our revised manuscript: “(2) The CNEMC network was built in 2013. Before 2013, the national observations of PM_{2.5} and O₃ concentrations were not available, which make it difficult to select the time and location of complex air pollution events and to evaluate the model results. Based on observation data, we were mainly focused on impacts of ARF and API on surface O₃ during complex air pollution episodes from 2014 to 2017. Additional simulations of High_PM, High_O₃, and Low_POL support the conclusion

obtained from the complex air pollution episodes that the reduction in O₃ by API is larger than that by ARF.”

Response to “*However, if the authors are at least aware of a high PM_{2.5} case from the 2001-2005 period it would be worth comparing that with the current HI_PM case to see if the magnitude of the API and ARF impacts have decreased in a significant way.*”

Thanks to the Reviewer’s suggestion. The comparison is limited by the availability of observational data, as we explained above.

Minor comments:

1. *Line 78: field not “filed”*

Response:

Changed.

2. *Line 84: Should the unit be $\mu\text{g m}^{-3}$ or ppb?*

Response:

The unit is $\mu\text{g m}^{-3}$ in Xing et al. (2017) paper.

3. *Line 206: done instead of “did”*

Response:

We have changed the “did” to “done” in the revised manuscript.

4. *Line 291: should be “was caused”*

Response:

Corrected.

5. *Line 414: How can API contribute more than 100% to a reduction in O₃? The word contribution implies “percent of” not “percent change”. If these values are a relative difference (i.e., percent change) then a word other than contribute needs to be used.*

Response:

We have revised the sentence as follows: “The changed meteorological variables and weakened photochemistry reaction further reduced surface-layer O₃ concentration by 10.0~11.4 ppb, with relative changes of 74.6%~106.5% by API and of -6.5%~25.4% by ARF.”

6. *Line 430: during “the” warm season*

Response:

Corrected.

References:

- Chen, L., Zhu, J., Liao, H., Yang, Y., and Yue, X.: Meteorological influences on PM_{2.5} and O₃ trends and associated health burden since China's clean air actions, *Sci. Total Environ.*, 744, <https://doi.org/10.1016/j.scitotenv.2020.140837>, 2020.
- Chinese State Council: Release of PM_{2.5} monitoring information in China, available at: http://www.gov.cn/jrzq/2013-01/01/content_2303447.htm, 2013 (in Chinese).
- Li, K., Jacob, D. J., Shen, L., Lu, X., De Smedt, I., and Liao, H.: Increases in surface ozone pollution in China from 2013 to 2019: anthropogenic and meteorological influences, *Atmos. Chem. Phys.*, 20, 11423–11433, <https://doi.org/10.5194/acp-20-11423-2020>, 2020.
- Xing, J., Wang, J. D., Mathur, R., Wang, S. X., Sarwar, G., Pleim, J., Hogrefe, C., Zhang, Y. Q., Jiang, J. K., Wong, D. and Hao, J. M.: Impacts of aerosol direct effects on tropospheric ozone through changes in atmospheric dynamics and photolysis rates, *Atmos. Chem. Phys.*, 17, 9869–9883, <https://doi.org/10.5194/acp-17-9869-2017>, 2017.

1 **Impacts of aerosol-photolysis interaction and aerosol-radiation**
2 **feedback on surface-layer ozone in North China during multi-**
3 **pollutant air pollution episodes**

4

5 Hao Yang¹, Lei Chen¹, Hong Liao¹, Jia Zhu¹, Wenjie Wang², Xin Li²

6

7 ¹Jiangsu Key Laboratory of Atmospheric Environment Monitoring and Pollution
8 Control, Jiangsu Collaborative Innovation Center of Atmospheric Environment and
9 Equipment Technology, School of Environmental Science and Engineering, Nanjing
10 University of Information Science & Technology, Nanjing 210044, China

11 ²State Joint Key Laboratory of Environmental Simulation and Pollution Control,
12 College of Environmental Sciences and Engineering, Peking University, Beijing
13 100871, China

14

15 **Correspondence:** Lei Chen (chenlei@nuist.edu.cn) and Hong Liao
16 (hongliao@nuist.edu.cn)

17

18 **Abstract**

19 We examined the impacts of aerosol-radiation interactions, including the effects of
20 aerosol-photolysis interaction (API) and aerosol-radiation feedback (ARF), on surface-
21 layer ozone (O₃) concentrations during four multi-pollutant air pollution episodes
22 characterized by high O₃ and PM_{2.5} levels during 28 July to 3 August 2014 (Episode1),
23 8-13 July 2015 (Episode2), 5-11 June 2016 (Episode3), and 28 June to 3 July 2017
24 (Episode4) in North China, by using the Weather Research and Forecasting with
25 Chemistry (WRF-Chem) model embedded with an integrated process analysis scheme.
26 Our results show that API and ARF reduced the daytime shortwave radiative fluxes at
27 the surface by 92.4~102.9 W m⁻² and increased daytime shortwave radiative fluxes in
28 the atmosphere by 72.8~85.2 W m⁻², as the values were averaged over the complex air
29 pollution areas (CAPAs) in each of the four episodes. As a result, the stabilized
30 atmosphere decreased the daytime planetary boundary layer height and 10 m wind
31 speed by 129.0~249.0 m and 0.05~0.15 m s⁻¹, respectively, in CAPAs in the four
32 episodes. Aerosols were simulated to reduce the daytime near-surface photolysis rates
33 of J[NO₂] and J[O¹D] by 1.8×10^{-3} ~ 2.0×10^{-3} s⁻¹ and 5.7×10^{-6} ~ 6.4×10^{-6} s⁻¹,
34 respectively, in CAPAs in the four episodes. All the four episodes show the same
35 conclusion that the reduction in O₃ by API is larger than that by ARF. API (ARF) was
36 simulated to change daytime surface-layer O₃ concentrations by -8.5 ppb (-2.9 ppb), -
37 10.3 ppb (-1.0 ppb), -9.1 ppb (-0.9 ppb) and -11.4 ppb (+0.7 ppb) in CAPAs of the four
38 episodes, respectively. Process analysis indicated that the weakened O₃ chemical
39 production made the greatest contribution to API effect, while the reduced vertical
40 mixing was the key process for ARF effect. Our conclusions suggest that future PM_{2.5}
41 reductions may lead to O₃ increases due to the weakened aerosol-radiation interactions,
42 which should be considered in air quality planning.

43

44 **1 Introduction**

45 The characteristics of air pollution in China during recent years are changing from
46 the single pollutant (e.g., PM_{2.5}, particulate matter with an aerodynamic equivalent
47 diameter of 2.5 μm or less) to multiple pollutants (e.g., PM_{2.5} and ozone (O₃)) (Zhao et
48 al., 2018; Zhu et al., 2019), and the synchronous occurrence of high PM_{2.5} and O₃
49 concentrations has been frequently observed, especially during the warm seasons (Dai
50 et al., 2021; Qin et al., 2021). Qin et al. (2021) reported that the co-occurrence of PM_{2.5}
51 and O₃ pollution days (days with PM_{2.5} concentration > 75 μg m⁻³ as well as maximum
52 daily 8 h average ozone concentration > 80 ppb) exceeded 324 days in eastern China
53 during 2015-2019. Understanding the complex air pollution is essential for making
54 plans to improve air quality in China.

55 Aerosols can influence O₃ by changing meteorology through absorbing and
56 scattering solar radiation (defined as aerosol-radiation feedback (ARF) in this work)
57 (Albrecht et al., 1989; Haywood et al., 2000; Lohmann et al., 2005), which influences
58 air quality by altering the chemical reactions, transport and deposition of the pollutant
59 (Gao et al., 2018; Qu et al., 2021; Xing et al., 2017; Zhang et al., 2018). Many studies
60 examined the feedback between aerosols and meteorology (Gao et al., 2015; Gao et al.,
61 2016a; Qiu et al., 2017; Chen et al., 2019; Zhu et al., 2021). For example, Gao et al.
62 (2015) used the WRF-Chem model to investigate the feedbacks between aerosols and
63 meteorological variables over the North China Plain in January 2013, and pointed out
64 that aerosols caused a decrease in surface temperature by 0.8-2.8 °C but an increase of
65 0.1-0.5 °C around 925 hPa. By using the same WRF-Chem model, Qiu et al. (2017)
66 reported that the surface downward shortwave radiation and PBLH were reduced by
67 54.6 W m⁻² and 111.4 m, respectively, due to aerosol direct radiative effect during 21-
68 27 February 2014 in the North China Plain. Such aerosol-induced changes in
69 meteorological fields are expected to influence O₃ concentrations during multi-
70 pollutant episodes with high concentrations of air pollutants.

71 Aerosols can also influence O₃ by altering photolysis rates (defined as aerosol-
72 photolysis interaction (API) in this work) (Dickerson et al., 1997; Liao et al., 1999; Li

73 et al., 2011; Lou et al., 2014). Dickerson et al. (1997) reported that the presence of pure
74 scattering aerosol increased ground level ozone in the eastern United States by 20 to 45
75 ppb, while the presence of strongly absorbing aerosol reduced ground level ozone by
76 up to 24 ppb. Wang et al. (2019) found that aerosols reduced the net ozone production
77 rate by 25% by reducing the photolysis frequencies during a comprehensive ~~field~~field
78 observation in Beijing in August 2012. Such aerosol-induced changes in photolysis
79 rates are expected to influence O₃ concentrations during multi-pollutant episodes with
80 high concentrations of air pollutants.

81 Few previous studies quantified the effects of ARF and API on O₃ concentrations.
82 Xing et al. (2017) applied a two-way online coupled WRF-CMAQ model and reported
83 that the combination of API and ARF reduced the surface daily maximum 1 h O₃
84 (MDA1 O₃) by up to 39 μg m⁻³ over China during January 2013. Qu et al. (2021) found,
85 by using the UK Earth System Model (UKESM1), that ARF reduced the annual average
86 surface O₃ by 3.84 ppb (14.9%) in the North China Plain during 2014. Gao et al. (2020)
87 analyzed the impacts of API on O₃ by using the WRF-Chem model and reported that
88 API reduced surface O₃ by 10.6 ppb (19.0%), 8.6 ppb (19.4%), and 8.2 ppb (17.7%) in
89 Beijing, Tianjin, and Shijiazhuang, respectively, during October 2018. However, these
90 previous studies mostly examined either ARF or API and did not examine their total
91 and respective roles in O₃ pollution in China. Furthermore, these previous studies
92 lacked process understanding about the impacts of ARF and API on O₃ pollution under
93 co-occurrence of PM_{2.5} and O₃ pollution events.

94 The present study aims to quantify the respective/combined impacts of ARF and
95 API on surface O₃ concentrations by using the WRF-Chem model, and to identify the
96 prominent physical and/or chemical processes responsible for ARF and API effects by
97 using an integrated process rate (IPR) analysis embedded in the WRF-Chem model. We
98 carry on simulations and analyses on four multi-pollutant air pollution episodes
99 (Episode1: 28 July to 3 August 2014; Episode2: 8-13 July 2015; Episode3: 5-11 June
100 2016; Episode4, 28 June to 3 July 2017) in North China with high O₃ and PM_{2.5} levels
101 (the daily mean PM_{2.5} and the maximum daily 8-h average O₃ concentration are larger

102 than $75 \mu\text{g m}^{-3}$ and 80 ppb, respectively). These episodes are selected because (1) these
103 events with high concentrations of both $\text{PM}_{2.5}$ and O_3 are the major subjects of air
104 pollution control, (2) high concentrations of both $\text{PM}_{2.5}$ and O_3 allow one to obtain the
105 strongest signals of ARF and API, (3) the measurements of $\text{J}[\text{NO}_2]$ during 2014 and
106 2015 from Peking University site (Wang et al., 2019) can help to constrain the simulated
107 photolysis rates of NO_2 , and (4) selected events cover different years of 2014 to 2017
108 during which the governmental Air Pollution Prevention and Control Action Plan was
109 implemented (the changes in emissions and observed $\text{PM}_{2.5}$ in the studied region during
110 2014-2017 are shown in Fig. S1). We expect that the conclusions obtained from
111 multiple episodes represent the general understanding of the impacts of ARF and API.

112 The model configuration, numerical experiments, observational data, and the
113 integrated process rate analysis are described in section 2. Section 3 shows the model
114 evaluation. Results and discussions are ~~presented~~exhibited in section 4, and the
115 conclusions ~~and discussions~~ are summarized~~provided~~ in section 5.

116 **2 Methods**

117 **2.1 Model configuration**

118 The version 3.7.1 of the online-coupled Weather Research and Forecasting with
119 Chemistry (WRF-Chem) model (Grell et al., 2005; Skamarock et al., 2008) is used in
120 this study to explore the impacts of aerosol-radiation interactions on surface-layer O_3
121 in North China. WRF-Chem can simulate gas phase species and aerosols coupled with
122 meteorological fields, and has been widely used to investigate air pollution over North
123 China (Gao et al., 2016a; Gao et al., 2020; Wu et al., 2020). As shown in Fig. 1, we
124 design two nested model domains with the number of grid points of 57 (west–east) \times
125 41 (south–north) and 37 (west–east) \times 43 (south–north) at 27 and 9 km horizontal
126 resolutions, respectively. The parent domain centers at (39 °N, 117 °E). The model
127 contains 29 vertical levels from the surface to 50 hPa, with 14 levels below 2 km for
128 the fully description of the vertical structure of planetary boundary layer (PBL).

129 The Carbon Bond Mechanism Z (CBM-Z) is selected as the gas-phase chemical
130 mechanism (Zaveri and Peters, 1999), and the full 8-bin MOSAIC (Model for

131 Simulating Aerosol Interactions and Chemistry) aerosol module with aqueous
132 chemistry is used to simulate aerosol evolution (Zaveri et al., 2008). The photolysis
133 rates are calculated by the Fast-J scheme (Wild et al., 2000). Other major physical
134 parameterizations used in this study are listed in Table 1.

135 The initial and boundary meteorological conditions are provided by the National
136 Centers for Environmental Prediction (NCEP) Final Analysis data with a spatial
137 resolution of $1^\circ \times 1^\circ$. In order to limit the model bias of simulated meteorological fields,
138 the four-dimensional data assimilation (FDDA) is used with the nudging coefficient of
139 3.0×10^{-4} for wind, temperature and humidity (no analysis nudging is applied for the
140 inner domain) (Lo et al., 2008; Otte, 2008). Chemical initial and boundary conditions
141 are obtained from the Model for Ozone and Related chemical Tracers, version 4
142 (MOZART-4) forecasts (Emmons et al., 2010).

143 Anthropogenic emissions in these four episodes are taken from the Multi-
144 resolution Emission Inventory for China (MEIC) (<http://www.meicmodel.org/>) (Li et
145 al., 2017a). These emission inventories provide emissions of sulfur dioxide (SO_2),
146 nitrogen oxides (NO_x), carbon monoxide (CO), non-methane volatile organic
147 compounds (NMVOCs), carbon dioxide (CO_2), ammonia (NH_3), black carbon (BC),
148 organic carbon (OC), PM_{10} (particulate matter with aerodynamic diameter is 10 μm and
149 less) and $\text{PM}_{2.5}$. Emissions are aggregated from four sectors, including power
150 generation, industry, residential, and transportation, with $0.25^\circ \times 0.25^\circ$ spatial
151 resolution. Biogenic emissions are calculated online by the Model of Emissions of
152 Gases and Aerosols from Nature (MEGAN) (Guenther et al., 2006).

153 **2.2 Numerical experiments**

154 To quantify the impacts of API and ARF on O_3 , three experiments have been
155 conducted: (1) BASE – the base simulation coupled with the interactions between
156 aerosol and radiation, which includes both impacts of API and ARF; (2) NOAPI – the
157 same as the BASE case, but the impact of API is turned off (aerosol optical properties
158 are set to zero in the photolysis module), following Wu et al. (2020); (3) NOALL – both
159 the impacts of API and ARF are turned off (removing the mass of aerosol species when

160 calculating aerosol optical properties in the optical module), following Qiu et al. (2017).
161 The differences between BASE and NOAPI (i.e., BASE minus NOAPI) represent the
162 impacts of API. The contributions from ARF can be obtained by comparing NOAPI and
163 NOALL (i.e., NOAPI minus NOALL). The combined effects of API and ARF on O₃
164 concentrations can be quantitatively evaluated by the differences between BASE and
165 NOALL (i.e., BASE minus NOALL).

166 All the experiments in Episode1, Episode2, Episode3 and Episode4 are conducted
167 from 26 July to 3 August 2014, 6-13 July 2015, 3-11 June 2016, and 26 June to 3 July
168 2017, respectively, with the first 40 hours as the model spin-up in each case. Simulation
169 results from the BASE cases of the four episodes are used to evaluate the model
170 performance.

171 **2.3 Observational data**

172 Simulation results are compared with meteorological and chemical measurements.
173 The surface-layer meteorological data (2 m temperature (T₂), 2 m relative humidity
174 (RH₂), and 10 m wind speed (WS₁₀)) with the temporal resolution of 3 h at ten stations
175 (Table S1) are obtained from NOAA's National Climatic Data Center
176 (<https://gis.ncdc.noaa.gov/maps/ncei/cdo/hourly>). The radiosonde data of temperature
177 at 08:00 and 20:00 LST in Beijing (39.93 °N, 116.28 °E) are provided by the University
178 of Wyoming (<http://weather.uwyo.edu/>). Observed hourly concentrations of PM_{2.5} and
179 O₃ at thirty-two sites (Table S2) in North China are collected from the China National
180 Environmental Monitoring Center (CNEMC). The photolysis rate of nitrogen dioxide
181 (J[NO₂]) measured at the Peking University site (39.99 °N, 116.31 °E) is also used to
182 evaluate the model performance. More details about the measurement technique of
183 J[NO₂] can be found in Wang et al. (2019). The aerosol optical depth (AOD) at Beijing
184 site (39.98°N, 116.38°E) is provided by AERONET (level 2.0,
185 <http://aeronet.gsfc.nasa.gov/>). The AOD at 675 nm and 440 nm are used to derive the
186 AOD at 550 nm to compare with the simulated ones.

187 **2.4 Integrated process rate analysis**

188 Integrated process rate (IPR) analysis has been widely used to quantify the
189 contributions of different processes to O₃ variations (Goncalves et al., 2009; Gao et al.,
190 2016b; Tang et al., 2017; Gao et al., 2018). In this study, four physical/chemical
191 processes are considered, including vertical mixing (VMIX), net chemical production
192 (CHEM), horizontal advection (ADVH), and vertical advection (ADVZ). VMIX is
193 initiated by turbulent process and closely related to PBL development, which influences
194 O₃ vertical gradients. CHEM represents the net O₃ chemical production (chemical
195 production minus chemical consumption). ADVH and ADVZ represent transport by
196 winds (Gao et al., 2016b). In this study, we define ADV as the sum of ADVH and ADVZ.

197 **3 Model evaluation**

198 Reasonable representation of observed meteorological and chemical variables by
199 the WRF-Chem model can provide foundation for evaluating the impacts of aerosols
200 on surface-layer ozone concentrations. The model results presented in this section are
201 taken from the BASE cases in the four episodes. The concentrations of air pollutants
202 are averaged over the thirty-two observation sites in Beijing, Tianjin and Baoding. To
203 ensure the data quality, the mean value for each time is calculated only when
204 concentrations are available at more than sixteen sites, as ~~did~~done in Li et al. (2019a).

205 **3.1 Chemical simulations**

206 Figure 2 shows the temporal variations of observed and simulated PM_{2.5} and O₃
207 concentrations over North China for the four episodes. As shown in Fig. 2, the temporal
208 variations of observed PM_{2.5} can be well performed by the model with index of
209 agreement (IOA) of 0.68, 0.68, 0.67 and 0.44 and normalized mean bias (NMB) of -
210 19.2%, 4.1%, 30.4% and 13.9% during Episode1, Episode2, Episode3 and Episode4,
211 respectively. The model also tracks well the diurnal variation of O₃ over the North
212 China, with IOA of 0.89, 0.94, 0.92 and 0.87 and NMB of -12.0%, -0.4%, 1.6% and -
213 13.8% for Episode1, Episode2, Episode3 and Episode4, respectively.

214 Figure S2 shows the correlation between observed and simulated AOD at 550 nm
215 in Beijing. In the WRF-Chem model, the AOD at 550 nm are calculated by using the

216 values at 400 and 600 nm according to the Angstrom exponent. Analyzing Fig. S2, the
217 model can reproduce the observed AOD with R of 0.7 and NMB of 7.9%.

218 **3.2 Meteorological simulations**

219 Figure 3 shows the time series of observed and simulated T_2 , RH_2 , WS_{10} and $J[NO_2]$
220 during the four episodes. The observed T_2 , RH_2 , WS_{10} are averaged over the ten
221 meteorological observation stations, and the $J[NO_2]$ are measured at Peking University.
222 Most of the monitored $J[NO_2]$ in Episode3 and Episode4 are unavailable, so the
223 comparison of $J[NO_2]$ in Episode3 and Episode4 is not shown. Generally, the model
224 can depict the temporal variations of T_2 fairly well with IOA of 0.94~0.98 and the mean
225 bias (MB) of -1.9~-0.6 °C. For RH_2 , the IOA and MB are 0.90~0.98 and -6.5%~1.9%,
226 respectively. Although WRF-Chem model overestimates WS_{10} with the MB of 0.6~1.0
227 $m s^{-1}$, the IOA for WS_{10} is 0.70~0.83 and the root-mean-square error (RMSE) is 0.9~1.5
228 $m s^{-1}$, which is smaller than the threshold of model performance criteria ($2 m s^{-1}$)
229 proposed by Emery et al. (2001). The positive bias in wind speed can also be reproduced
230 in other studies (Zhang et al., 2010; Gao et al., 2015; Liao et al., 2015; Qiu et al., 2017).
231 The predicted $J[NO_2]$ agrees well with the observations with IOA of 0.98~0.99 and
232 NMB of 6.8%~6.9%. We also conduct comparisons of observed and simulated
233 temperature profiles at 08:00 and 20:00 LST in Beijing during the four episodes (Fig.
234 S3). The vertical profiles of observed temperature can be well captured by the model in
235 these four complex air pollution episodes. Generally, the WRF-Chem model can
236 reasonably reproduce the temporal variations of observed meteorological parameters.

237 **4 Results**

238 We examine the impacts of aerosol-radiation interactions on O_3 concentrations
239 with a special focus on the complex air pollution areas (CAPAs, Fig. S4) in the four
240 episodes, where the daily mean simulated $PM_{2.5}$ and MDA8 (maximum daily 8-h
241 average) O_3 concentrations are larger than $75 \mu g m^{-3}$ and 80 ppb, respectively, based
242 on the National Ambient Air Quality Standards (<http://www.mee.gov.cn>).

243 **4.1 Impacts of aerosol-radiation interactions on meteorology**

244 Figure 4 shows the impacts of aerosol-radiation interactions on shortwave
245 radiation at the surface (BOT_SW), shortwave radiation in the atmosphere (ATM_SW),
246 PBLH, and WS₁₀ during the daytime (08:00-17:00 LST) from Episode1 to Episode4.
247 Analyzing the results of the interactions between aerosol and radiation (the combined
248 impacts of API and ARF), BOT_SW is decreased over the entire simulated domain in
249 the four episodes with the decreases of 93.2 W m⁻² (20.5%), 100.3 W m⁻² (19.5%), 92.4
250 W m⁻² (19.2%) and 102.9 W m⁻² (20.7%) over CAPAs, respectively. Contrary to the
251 changes in BOT_SW, ATM_SW is increased significantly in the four episodes with the
252 increases of 72.8 W m⁻² (25.3%), 85.2 W m⁻² (29.0%), 73.7 W m⁻² (26.4%) and 76.9 W
253 m⁻² (25.8%) over CAPAs, respectively. The decreased BOT_SW perturbs the near-
254 surface energy flux, which weakens convection and suppresses the development of PBL
255 (Li et al., 2017b). The mean PBLHs over CAPAs are decreased by 129.0 m (13.0%),
256 249.0 m (20.9%), 224.6 m (19.0%) and 227.0 m (20.9%), respectively. WS₁₀ exhibits
257 overall reductions over CAPAs and is calculated to decrease by 0.12 m s⁻¹ (3.6%), 0.05
258 m s⁻¹ (1.6%), 0.12 m s⁻¹ (3.0%) and 0.15 m s⁻¹ (4.3%), for the four episodes, respectively.
259 We also examine the changed meteorological variables caused by API and ARF
260 respectively. As shown in Fig. S5 and S6, API has little impact on meteorological
261 variables; which means the major contributor to the meteorology variability is ARF.

262 4.2 Impacts of aerosol-radiation interactions on photolysis

263 Figure 5 shows the spatial distributions of mean daytime surface-layer PM_{2.5}
264 concentrations simulated by BASE cases and the changes in J[NO₂] and J[O¹D] due to
265 aerosol-radiation interactions from Episode1 to Episode4. When the combined impacts
266 (API and ARF) are considered, J[NO₂] and J[O¹D] are decreased over the entire domain
267 in the four episodes, and the spatial patterns of changed J[NO₂] and J[O¹D] are similar
268 to that of simulated PM_{2.5}. Analyzing the four simulated episodes, the surface J[NO₂]
269 averaged over CAPAs are decreased by $1.8 \times 10^{-3} \text{ s}^{-1}$ (40.5%), $2.0 \times 10^{-3} \text{ s}^{-1}$ (36.8%),
270 $1.8 \times 10^{-3} \text{ s}^{-1}$ (36.0%), and $2.0 \times 10^{-3} \text{ s}^{-1}$ (38.0%), respectively. The decreased surface
271 J[O¹D] over CAPAs are $6.1 \times 10^{-6} \text{ s}^{-1}$ (48.8%), $6.3 \times 10^{-6} \text{ s}^{-1}$ (41.4%), $5.7 \times 10^{-6} \text{ s}^{-1}$
272 (44.6%), and $6.4 \times 10^{-6} \text{ s}^{-1}$ (46.9%), respectively. Figure S7 exhibits the impacts of API

273 and ARF on surface $J[\text{NO}_2]$ and $J[\text{O}^1\text{D}]$. Conclusions can be summarized that $J[\text{NO}_2]$
274 and $J[\text{O}^1\text{D}]$ are significantly modified by API and little affected by ARF.

275 **4.3 Impacts of aerosol-radiation interactions on O_3**

276 Figure 6 shows the changes in surface-layer O_3 due to API, ARF, and the combined
277 effects (denoted as ALL) from Episode1 to Episode4. As shown in Fig. 6(a1-a4), API
278 alone leads to overall surface O_3 decreases over the entire domain with average
279 reductions of 8.5 ppb (10.2%), 10.3 ppb (11.8%), 9.1 ppb (11.2%), and 11.4 ppb (12.2%)
280 over CAPAs in the four episodes, respectively. The changes can be explained by the
281 substantially diminished UV radiation due to aerosol loading, which significantly
282 weakens the efficiency of photochemical reactions and restrains O_3 formation. However,
283 the decreased surface O_3 concentrations due to ARF are only 2.9 ppb (3.2%, Fig. 6(b1)),
284 1.0 ppb (1.1%, Fig. 6(b2)) and 0.9 ppb (1.0%, Fig. 6(b3)) for the Episode1 to Episode3
285 but ARF increased surface O_3 concentrations by 0.7 ppb (0.5%, Fig.6(b4)) during
286 Episode4, which was caused by the enhancement of chemical production (Fig. S10 and
287 Section 4.4). All the episodes show same conclusion that the reduction in O_3 by API is
288 larger than that by ARF. Fig. 6(c1-c4) presents the combined effects of API and ARF.
289 Generally, aerosol-radiation interactions decrease the surface O_3 concentrations by 11.4
290 ppb (13.7%), 11.3 ppb (13.0%), 10.0 ppb (12.3%) and 10.7 ppb (11.6%) averaged over
291 CAPAs in the four episodes, respectively.

292 **4.4 Influencing mechanism of aerosol-radiation interactions on O_3**

293 Figure 7a shows mean results of the four episodes (Episode1, Episode2, Episode3
294 and Episode4) in diurnal variations of simulated daytime surface-layer O_3
295 concentrations from BASE, NOAPI and NOALL cases averaged over CAPAs. All the
296 experiments (BASE, NOAPI and NOALL) present O_3 increases from 08:00 LST. It is
297 shown that the simulated O_3 concentrations in BASE case increase more slowly than
298 that in NOAPI and NOALL cases. To explain the underlying mechanisms of API and
299 ARF impacts on O_3 , we quantify the variations in contributions of different processes
300 (ADV, CHEM, and VMIX) to O_3 by using the IPR analysis.

301 Figure 7b shows hourly surface O_3 changes induced by each physical/chemical

302 process (i.e., ADV, CHEM, and VMIX) in BASE case averaged from Episode1 to
303 Episode4. The significant positive contribution to the hourly variation in O₃ is
304 contributed by VMIX, and the contribution reaches the maximum at about 09:00 LST.
305 Since VMIX increases the surface O₃ concentrations by transporting O₃ from aloft
306 (where O₃ concentrations are high) to the surface layer (Tang et al., 2017; Xing et al.,
307 2017; Gao et al., 2018). The CHEM process makes negative contributions at around
308 09:00 and 16:00 LST, which means that the chemical consumption of O₃ is stronger
309 than the chemical production. At noon, the net chemical contribution turns to be
310 positive due to stronger solar UV radiation. The contribution from all the processes
311 (NET, the sum of VMIX, CHEM, and ADV) to O₃ variation is peaked at the noon and
312 then becomes weakened. After sunset (17:00 LST), the NET contribution turns to be
313 negative over CAPAs, leading to O₃ decrease.

314 Figure 7c shows the changes in hourly process contributions caused by API
315 averaged from Episode1 to Episode4. The chemical production of O₃ is suppressed
316 significantly due to aerosol impacts on photolysis rates. The weakened O₃ chemical
317 production decreases the contribution from CHEM, and results in a negative value of
318 CHEM_DIF (-3.44 ppb h⁻¹). In contrast to CHEM_DIF, the contribution from changed
319 VMIX (VMIX_DIF) to O₃ concentration due to API is always positive, and the mean
320 value is +3.26 ppb h⁻¹. The positive change in VMIX due to API may be associated with
321 the different vertical gradient of O₃ between BASE and NOAPI cases (Gao et al., 2020),
322 as shown in Fig. 8a. The impact of API on ADV process is relatively small (-0.26 ppb
323 h⁻¹). NET_DIF, namely the sum of VMIX_DIF, CHEM_DIF and ADV_DIF, indicates
324 the differences in hourly O₃ changes caused by API. As shown in Fig. 7c, NET_DIF is
325 almost negative during the daytime over CAPAs with the mean value of -0.44 ppb h⁻¹.
326 This is because the decreases in CHEM and ADV are larger than the increases in VMIX
327 caused by API; the O₃ decrease is mainly attributed to the significantly decreased
328 contribution from CHEM. The maximum difference in O₃ between BASE and NOAPI
329 appears at 11:00 LST with a value of -12.5 ppb (Fig. 7a).

330 Figure 7d shows the impacts of ARF on each physical/chemical process

331 contribution to the hourly O₃ variation averaged from Episode1 to Episode4. At 08:00
332 LST, the change in VMIX due to ARF is large with a value of -3.5 ppb h⁻¹, resulting in
333 a net negative variation with all processes considered. The decrease in O₃ reaches the
334 maximum with the value of 5.0 ppb at around 08:00 LST over CAPAs (Fig. 7a). During
335 09:00 to 16:00 LST, the positive VMIX_DIF (mean value of +0.10 ppb h⁻¹) or the
336 positive CHEM_DIF (mean value of +0.75 ppb h⁻¹) is the major process to positive
337 NET_DIF. The positive VMIX_DIF is related to the evolution in boundary layer during
338 the daytime. The VOCs/NO_x ratio is calculated to classify sensitivity regimes and to
339 indicate the possible O₃ responses to changes in VOCs and/or NO_x concentrations. O₃
340 production is VOC-limited if the ratio is less than 4, and is NO_x-limited if the ratio is
341 larger than 15 (Edson et al., 2017; Li et al., 2017c). The ratio of VOCs/NO_x ranging
342 around 4-15 indicates a transitional regime, where ozone is nearly equally sensitive to
343 both species (Sillman, 1999). As shown in Fig. S8, (a-f), O₃ is mainly formed under the
344 VOC-limited and the transition regimes in CAPAs. As shown in Figs. S8(g-i) and S8(j-
345 l), both the surface concentrations of VOCs and NO_x are increased when the impacts of
346 ARF are considered. Thus, the contribution of CHEM in NOAPI is larger than that in
347 NOALL.

348 When both impacts of API and ARF are considered, the variation pattern of the
349 difference in hourly process contribution shown in Fig. 7e is similar to that in Fig. 7c,
350 which indicates that API is the dominant factor to surface-layer O₃ reduction.

351 Figure 8 presents the vertical profiles of simulated daytime O₃ concentrations in
352 three cases (BASE, NOAPI, and NOALL), and the differences in contributions from
353 each physical/chemical process to hourly O₃ variations caused by API, ARF and the
354 combined effects averaged over CAPAs from Episode1 to Episode4. As shown in Fig.
355 8a, the O₃ concentration is lower in BASE than that in other two scenarios (NOAPI and
356 NOALL), especially at the lower 12 levels (below 801.8 m), owing to the impacts of
357 aerosols (API and/or ARF).

358 The changes in each process contribution caused by API are presented in Fig. 8b.
359 The contribution from CHEM_DIF is -2.1 ppb h⁻¹ for the first seven layers (from 25.6

360 to 318.5 m). Conversely, the contribution from VMIX_DIF shows a positive value
361 under the 318.5 m (between the first layer to the seventh layer) with the mean value of
362 +1.8 ppb h⁻¹. The positive variation in VMIX due to API may be associated with the
363 different vertical gradient of O₃ between BASE and NOAPI again. The contributions
364 of changed advections (ADVH_DIF and ADVZ_DIF) are relatively small, with mean
365 values of +0.03 and -0.18 ppb h⁻¹ below the first seven layers, which may result from
366 small impact of API on wind field (Fig. S6(a4-d4)). The net difference is a negative
367 value (-0.45 ppb h⁻¹); API leads to O₃ reduction not only nearly surface but also aloft.

368 Figure 8c shows the differences in O₃ budget due to ARF. When the ARF is
369 considered, the vertical turbulence is weakened and the development of PBL is
370 inhibited, which makes VMIX_DIF negative at the lower seven layers (below the 318.5
371 m) with a mean value of -0.69 ppb h⁻¹, but the variation in CHEM caused by ARF is
372 positive with a mean value of +0.86 ppb h⁻¹. The enhanced O₃ precursors due to ARF
373 can promote the chemical production of O₃ (Tie et al., 2009; Gao et al., 2018). The
374 changes of ADVZ and ADVH (ADVZ_DIF and ADVH_DIF) caused by ARF are
375 associated with the variations in wind field. When ARF is considered, the horizontal
376 wind speed is decreased (Fig. S9(a)), which makes ADVH_DIF positive at the lower
377 twelve layers with a mean value of +0.30 ppb h⁻¹. However, ADVZ_DIF is negative at
378 these layers with a mean value of -0.26 ppb h⁻¹ because aerosol radiative effects
379 decrease the transport of O₃ from the upper to lower layers (Fig. S9(b)).

380 In Fig. 8d, the pattern and magnitude of the differences in process contributions
381 between BASE and NOALL are similar to those caused by API, indicating the dominate
382 contributor of API on O₃ changes. The impacts of API on O₃ both near the surface and
383 aloft are greater than those of ARF.

384 Figure S10 and S11 detailed show the influencing mechanism of aerosol-radiation
385 interactions on O₃ in each episode. Similar variation characteristics can be found among
386 the four episodes as the mean situation discussed above, with the larger impacts of API
387 on O₃ both near the surface and aloft than those of ARF, indicating the role of API is
388 much larger than that of ARF during all the simulated episodes.

389 4.5 Discussions

390 We presented above the results from our simulations of multi-pollutant air
391 pollution episodes. In order to make the conclusion be more general, we carried out
392 simulations for three additional air pollution conditions, i.e., (1) PM_{2.5} pollution alone
393 (High PM, with daily mean PM_{2.5} concentration larger than 75 μg m⁻³), (2) O₃ pollution
394 alone (High O₃, with the maximum daily 8-h average O₃ concentration larger than 80
395 ppb), and (3) neither PM_{2.5} nor O₃ exceeded air quality standard (Low POL, with daily
396 mean PM_{2.5} and the maximum daily 8-h average O₃ concentrations smaller than 75 μg
397 m⁻³ and 80 ppb, respectively). For each condition of air pollution, we examined two
398 episodes.

399 Figures S12 and S13 show the temporal variations of observed and simulated
400 PM_{2.5} and O₃ concentrations during 7-12 October 2014 (High PM Episode1), 7-11
401 April 2014 (High PM Episode2), 15-21 June 2017 (High O₃ Episode1), 12-17 July
402 2017 (High O₃ Episode2), 13-18 June 2016 (Low POL Episode1), and 13-17 July
403 2016 (Low POL Episode2). The temporal variations of observed PM_{2.5} can be well
404 captured by the model with IOAs of 0.63, 0.82, 0.56, 0.42, 0.76 and 0.54, and NMBs
405 of 7.4%, 20.3%, -21.7%, -25.9%, 14.7% and -29.3% during High PM Episode1,
406 High PM Episode2, High O₃ Episode1, High O₃ Episode2, Low POL Episode1,
407 and Low POL Episode2, respectively. The model also simulates well the diurnal
408 variation of O₃ over the North China, with IOAs of 0.87, 0.80, 0.87, 0.90, 0.84 and 0.86,
409 and NMBs of -9.4%, -29.5%, -15.2%, -9.4%, 11.6% and 18.0% in these six episodes,
410 respectively.

411 Figure 9 shows changes in daytime surface-layer O₃ due to API, ARF, and the
412 combined effects (denoted as ALL) of High PM Episode1, High PM Episode2,
413 High O₃ Episode1, High O₃ Episode2, Low POL Episode1, and
414 Low POL Episode2. As summarized in Table 2, all the simulations confirm the same
415 conclusion that the reduction in O₃ by API is larger than that by ARF. Averaged over
416 the entire domain, the percentage reductions in O₃ by API and ARF are, respectively,
417 29.3% and 6.2% in High PM Episode1, 16.9% and 4.7% in High PM Episode2, 5.3%

418 and 0.1% in High_O₃_Episode1, 4.5% and 0.1% in High_O₃_Episode2, 6.8% and 1.0%
419 in Low_POL_Episode1, and 2.9% and 0.7% in Low_POL_Episode2. It's worth noting
420 that the percentage reductions in O₃ from both API and ARF in High_PM episodes are
421 1.6~3.2 times the impacts in the complex episodes, while the impacts in cases of
422 Low_POL and High_O₃ are 0.3~0.7 times the impacts of complex episodes."

423 **5 Conclusions and Discussions**

424 In this study, the fully coupled regional chemistry transport model WRF-Chem is
425 applied to investigate the impacts of aerosol-radiation interactions, including the
426 impacts of aerosol-photolysis interaction (API) and the impacts of aerosol-radiation
427 feedback (ARF), on O₃ during summertime complex air pollution episodes during 28
428 July to 3 August 2014 (Episode1), 8-13 July 2015 (Episode2), 5-11 June 2016
429 (Episode3) and 28 June to 3 July 2017 (Episode4). Three sensitivity experiments are
430 designed to quantify the respective and combined impacts from API and ARF. Generally,
431 the spatiotemporal distributions of observed pollutant concentrations and
432 meteorological parameters can be captured fairly well by the model with index of
433 agreement of 0.44~0.94 for pollutant concentrations and 0.70~0.99 for meteorological
434 parameters.

435 Sensitivity experiments show that aerosol-radiation interactions decrease
436 BOT_SW, WS₁₀, PBLH, J[NO₂], and J[O¹D] by 92.4~102.9 W m⁻², 0.05~0.15 m s⁻¹,
437 129.0~249.0 m, 1.8×10^{-3} ~ 2.0×10^{-3} s⁻¹, and 5.7×10^{-6} ~ 6.4×10^{-6} s⁻¹ over CAPAs, and
438 increase ATM_SW by 72.8~85.2 W m⁻², respectively. The changed meteorological
439 variables and weakened photochemistry reaction further reduce surface-layer O₃
440 concentrations by ~~up to~~ 10.0~11.4 ppb, with relative changes of 74.6%~106.5% by API
441 and ~~of -6.5%~25.4% by ARF~~ ~~contributing 74.6%~106.5% and -6.5%~-25.4%,~~
442 respectively.

443 We further examine the influencing mechanism of aerosol-radiation interactions
444 on O₃ by using integrated process rate analysis. API can directly affect O₃ by reducing
445 the photochemistry reactions within the lower several hundred meters and therefore
446 amplify the O₃ vertical gradient, which promotes the vertical mixing of O₃. The reduced

447 photochemistry reactions of O₃ weaken the chemical contribution and reduce surface
448 O₃ concentrations, even though the enhanced vertical mixing can partly counteract the
449 reduction. ARF affects O₃ concentrations indirectly through the changed
450 meteorological variables, e.g., the decreased PBLH. The suppressed PBL can weaken
451 the vertical mixing of O₃ by turbulence. Generally, the impacts of API on O₃ both near
452 the surface and aloft are greater than those of ARF, indicating the dominant role of API
453 on O₃ reduction related with aerosol-radiation interactions.

454 This study provides a detailed understanding of aerosol impacts on O₃ through
455 aerosol-radiation interactions (including both API and ARF), with the general
456 conclusion summarized as follows: when the impacts of aerosol-radiation interactions
457 are considered, the changed meteorological variables and weakened photochemistry
458 reaction can change surface-layer O₃ concentrations during the warm season, and the
459 API is the dominant factor for O₃ reduction. The results can also imply that future PM_{2.5}
460 reductions may lead to O₃ increases due to weakened aerosol-radiation interactions. A
461 recent study emphasized the need for controlling VOCs emissions to mitigate O₃
462 pollution (Li et al., 2019b). Therefore, tighter controls of O₃ precursors (especially
463 VOCs emissions) are needed to counteract future O₃ increases caused by weakened
464 aerosol-radiation interactions.

465 There are some limitations in this work. (1) In the current CBMZ and MOSAIC
466 schemes, the formation of SOA (secondary organic aerosol) is not included (Gao et al.,
467 2015; Chen et al., 2019). The absence of SOA can underestimate the impacts of API
468 and ARF on O₃. Meanwhile, the lack of SOA may lead to weaker heterogeneous
469 reactions to result in higher O₃ concentrations (Li et al., 2019c). The net effect of the
470 two processes will be discussed and quantified in our future study. (2) The CNEMC
471 network was built in 2013. Before 2013, the national observations of PM_{2.5} and O₃
472 concentrations were not available, which make it difficult to select the time and area of
473 complex air pollution events and to evaluate the model results. Based on observation
474 data, we were mainly focused on impacts of ARF and API on surface O₃ during complex
475 air pollution episodes from 2014 to 2017. Additional simulations of High PM, High O₃,

476 and Low_POL support the conclusion obtained from the complex air pollution episodes
477 that the reduction in O₃ by API is larger than that by ARF.

478
479 There are some limitations in this work:—

480 (1) In the current CBMZ and MOSAIC schemes, the formation of SOA (secondary
481 organic aerosol) is not included (Gao et al., 2015; Chen et al., 2019). The absence
482 of SOA can underestimate the impacts of API and ARF on O₃. Meanwhile, the lack
483 of SOA may lead to weaker heterogeneous reactions to result in higher O₃
484 concentrations (Li et al., 2019c). The net effect of the two processes will be
485 discussed and quantified in our future study.—

486 (2) We presented above the results from our simulations of multi-pollutant air pollution
487 episodes. In order to show that the conclusion of this work can be applied to other
488 conditions of air pollution, three additional situations are carried out, i.e., (1) PM_{2.5}
489 pollution alone (Episode_add1, the daily mean PM_{2.5} concentration is larger than
490 75 μg m⁻³), (2) neither PM_{2.5} nor O₃ exceed air quality standard (Episode_add2,
491 the daily mean PM_{2.5} and maximum daily 8-h average O₃ concentration are smaller
492 than 75 μg m⁻³ and 80 ppb, respectively), and (3) O₃ pollution alone
493 (Episode_add3, the maximum daily 8-h average O₃ concentration is larger than 80
494 ppb). Detailed information about these three additional episodes is listed in the
495 supporting information (Text S1 and Table S3). Analyzing Episode_add1,
496 Episode_add2 and Episode_add3 in Fig. S13, API alone is simulated to reduce
497 surface O₃ averaged over each episode and over the entire domain by 15.3 ppb
498 (29.3%), 4.4 ppb (6.8%) and 4.5 ppb (5.3%), respectively, and ARF alone reduces
499 surface O₃ by 3.9 ppb (6.2%), 0.6 ppb (1.0%), and 0.1 ppb (0.1%), respectively.
500 All the results confirm the same conclusion that the reduction in O₃ by API is
501 larger than that by ARF.

502

503 **Data availability**

504 The observed hourly surface concentrations of air pollutants are derived from the China
505 National Environmental Monitoring Center (<http://www.cnemc.cn>). The observed
506 surface meteorological data are obtained from NOAA's National Climatic Data Center
507 (<https://gis.ncdc.noaa.gov/maps/ncei/cdo/hourly>). The radiosonde data are provided by
508 the University of Wyoming (<http://weather.uwyo.edu/>). The photolysis rates of nitrogen
509 dioxide in Beijing are provided by Xin Li (li_xin@pku.edu.cn). The aerosol optical
510 depth in Beijing is obtained from the AERONET level 2.0 data collection
511 (<http://aeronet.gsfc.nasa.gov/>). The simulation results can be accessed by contacting
512 Lei Chen (chenlei@nuist.edu.cn) and Hong Liao (hongliao@nuist.edu.cn).

513

514 **Author contributions**

515 HY, LC, and HL conceived the study and designed the experiments. HY and LC
516 performed the simulations and carried out the data analysis. JZ, WW, and XL provided
517 useful comments on the paper. HY, LC, and HL prepared the paper with contributions
518 from all co-authors.

519

520 **Competing interests**

521 The authors declare that they have no competing interests.

522

523 **Acknowledgements**

524 This work is supported by the National Key R&D Program of China
525 (2019YFA0606804), the National Natural Science Foundation of China (42007195),
526 the Meteorological Soft Science Program of China Meteorological Administration
527 (2021ZZXM46), and the Postgraduate Research and Practice Innovation Program of
528 Jiangsu Province (KYCX21_1014). We acknowledge the High Performance
529 Computing Center of Nanjing University of Information Science & Technology for
530 their support of this work.

531 **Reference**

532 Albrecht, B. A.: Aerosols, cloud microphysics, and fractional cloudiness, *Science*, 245,
533 1227–1230, 1989.

534 Chen, F. and Dudhia, J.: Coupling an Advanced Land Surface – Hydrology Model with
535 the Penn State – NCAR MM5 Modeling System. Part I: Model Implementation and
536 Sensitivity, *Mon. Weather Rev.*, 129(4), 569–585, 2001.

537 Chen, L., Zhu, J., Liao, H., Gao, Y., Qiu, Y., Zhang, M., Liu, Z., Li, N., and Wang, Y.:
538 Assessing the formation and evolution mechanisms of severe haze pollution in the
539 Beijing–Tianjin–Hebei region using process analysis, *Atmos. Chem. Phys.*, 19,
540 10845–10864, <https://doi.org/10.5194/acp-19-10845-2019>, 2019.

541 Dai, H., Zhu, J., Liao, H., Li, J., Liang, M., Yang, Y., and Yue, X.: Co-occurrence of
542 ozone and PM_{2.5} pollution in the Yangtze River Delta over 2013–2019:
543 Spatiotemporal distribution and meteorological conditions, *Atmos. Res.*, 249,
544 105363, 2021.

545 Dickerson, R. R., Kondragunta, S., Stenchikov, G., Civerolo, K. L., Doddridge, B. G.,
546 and Holben, B. N.: The impact of aerosols on solar ultraviolet radiation and
547 photochemical smog, *Science*, 278, 827–830, [10.1126/science.278.5339.827](https://doi.org/10.1126/science.278.5339.827), 1997.

548 Edson, C. T., Ivan, H.-P. and Alberto, M.: Use of combined observational- and model-
549 derived photochemical indicators to assess the O₃-NO_x-VOC System sensitivity in
550 urban areas, *Atmosphere.*, 8, 22. <https://doi.org/10.3390/atmos8020022>, 2017.

551 Emery, C., Tai, E., and Yarwood, G.: Enhanced meteorological modeling and
552 performance evaluation for two Texas ozone episodes, in: Prepared for the Texas
553 Natural Resource Conservation Commission, ENVIRON International Corporation,
554 Novato, CA, USA, 2001.

555 Emmons, L. K., Walters, S., Hess, P. G., Lamarque, J.-F., Pfister, G. G., Fillmore, D.,
556 Granier, C., Guenther, A., Kinnison, D., Laepple, T., Orlando, J., Tie, X., Tyndall,
557 G., Wiedinmyer, C., Baughcum, S. L., and Kloster, S.: Description and evaluation of
558 the Model for Ozone and Related chemical Tracers, version 4 (MOZART-4), *Geosci.*
559 *Model Dev.*, 3, 43–67, [doi:10.5194/gmd-3-43-2010](https://doi.org/10.5194/gmd-3-43-2010), 2010.

560 Foken, T.: 50 years of the Monin-Obukhov similarity theory, *Bound.-Layer Meteor.*,
561 119, 431–437, 2006.

562 Gao, J., Li, Y., Zhu, B., Hu, B., Wang, L., and Bao, F.: What have we missed when
563 studying the impact of aerosols on surface ozone via changing photolysis rates?,
564 *Atmos. Chem. Phys.*, 20, 10831–10844, [https://doi.org/10.5194/acp-20-10831-](https://doi.org/10.5194/acp-20-10831-2020)
565 2020, 2020.

566 Gao, J. H., Zhu, B., Xiao, H., Kang, H. Q., Pan, C., Wang, D. D., and Wang, H. L.:
567 Effects of black carbon and boundary layer interaction on surface ozone in Nanjing,
568 China, *Atmos. Chem. Phys.*, 18, 7081–7094, [https://doi.org/10.5194/acp-18-7081-](https://doi.org/10.5194/acp-18-7081-2018)
569 2018, 2018.

570 Gao, M., Carmichael, G. R., Wang, Y., Saide, P. E., Yu, M., Xin, J., Liu, Z., and Wang,
571 Z.: Modeling study of the 2010 regional haze event in the North China Plain, *Atmos.*
572 *Chem. Phys.*, 16, 1673–1691, doi:10.5194/acp-16-1673-2016, 2016a.

573 Gao, J., Zhu, B., Xiao, H., Kang, H., Hou, X., and Shao, P.: A case study of surface
574 ozone source apportionment during a high concentration episode, under frequent
575 shifting wind conditions over the Yangtze River Delta, China, *Sci. Total Environ.*,
576 544, 853, <https://doi.org/10.1016/j.scitotenv.2015.12.039>, 2016b.

577 Gao, Y., Zhang, M., Liu, Z., Wang, L., Wang, P., Xia, X., Tao, M., and Zhu, L.:
578 Modeling the feedback between aerosol and meteorological variables in the
579 atmospheric boundary layer during a severe fog–haze event over the North China
580 Plain, *Atmos. Chem. Phys.*, 15, 4279–4295, doi:10.5194/acp-15-4279-2015, 2015.

581 Goncalves, M., Jimenez-Guerrero, P., Baldasano, J.M.: Contribution of atmospheric
582 processes affecting the dynamics of air pollution in South-Western Europe during a
583 typical summertime photochemical episode, *Atmos. Chem. Phys.*, 9, 849–864,
584 doi:10.5194/acp-9-849-2009, 2009.

585 Grell, G. A., Peckham, S. E., Schmitz, R., Mckeen, S. A., Frost, G., Skamarock, K.,
586 and Eder, B.: Fully coupled “online” chemistry within the WRF model, *Atmos.*
587 *Environ.*, 39, 6957–6975, 2005.

588 Guenther, A., Karl, T., Harley, P., Wiedinmyer, C., Palmer, P. I., and Geron, C.:

589 Estimates of global terrestrial isoprene emissions using MEGAN (Model of
590 Emissions of Gases and Aerosols from Nature), *Atmos. Chem. Phys.*, 6, 3181–3210,
591 doi:10.5194/acp-6-3181-2006, 2006.

592 Haywood, J. and Boucher, O.: Estimates of the direct and indirect radiative forcing due
593 to tropospheric aerosols: A review, *Rev. Geophys.*, 38, 513–543, 2000.

594 Hong, S.-Y., Noh, Y., and Dudhia, J.: A New Vertical Diffusion Package with an
595 Explicit Treatment of Entrainment Processes, *Mon. Weather Rev.*, 134, 2318–2341,
596 2006.

597 Iacono, M. J., Delamere, J. S., Mlawer, E. J., Shephard, M. W., Clough, S. A., and
598 Collins, W. D.: Radiative forcing by long-lived greenhouse gases: Calculations with
599 the AER radiative transfer models, *J. Geophys. Res.*, 113, D13103,
600 doi:10.1029/2008JD009944, 2008.

601 Li, G., Bei, N., Tie, X., and Molina, L. T.: Aerosol effects on the photochemistry in
602 Mexico City during MCMA-2006/MILAGRO campaign, *Atmos Chem Phys*, 11,
603 5169-5182, 10.5194/acp-11-5169-2011, 2011.

604 Li, J. D., Liao, H., Hu, J. L., Li, N.: Severe particulate pollution days in China during
605 2013-2018 and the associated typical weather patterns in Beijing-Tianjin-Hebei and
606 the Yangtze River Delta regions, *Environmental Pollution*, 248, 74-81, 2019a.

607 Li, K., Jacob, D. J., Liao, H., Zhu, J., Shah, V., Shen, L., Bates, K. H., Zhang, Q., and
608 Zhai, S.: A two-pollutant strategy for improving ozone and particulate air quality in
609 China, *Nat. Geosci.*, 12, 906–910, <https://doi.org/10.1038/s41561-019-0464-x>,
610 2019b.

611 Li, K., Jacob, D. J., Liao, H., Shen, L., Zhang, Q., and Bates, K. H.: Anthropogenic
612 drivers of 2013–2017 trends in summer surface ozone in China, *P. Natl. Acad. Sci.*
613 *USA*, 116, 422–427, <https://doi.org/10.1073/pnas.1812168116>, 2019c.

614 Li, M., Zhang, Q., Kurokawa, J.-I., Woo, J.-H., He, K., Lu, Z., Ohara, T., Song, Y.,
615 Streets, D. G., Carmichael, G. R., Cheng, Y., Hong, C., Huo, H., Jiang, X., Kang, S.,
616 Liu, F., Su, H., and Zheng, B.: MIX: a mosaic Asian anthropogenic emission
617 inventory under the international collaboration framework of the MICS-Asia and

618 HTAP, *Atmos. Chem. Phys.*, 17, 935–963, <https://doi.org/10.5194/acp-17-935-2017>,
619 2017a.

620 Li, Z., Guo, J., Ding, A., Liao, H., Liu, J., Sun, Y., Wang, T., Xue, H., Zhang, H., and
621 Zhu, B.: Aerosol and boundary-layer interactions and impact on air quality, *Nat. Sci.*
622 *Rev.*, 4, 810–833, <https://doi.org/10.1093/nsr/nwx117>, 2017b.

623 Li, K., Chen, L., Ying, F., White, S. J., Jang, C., Wu, X., Gao, X., Hong, S., Shen, J.,
624 Azzi, M. and Cen, K: Meteorological and chemical impacts on ozone formation: a
625 case study in Hangzhou, China, *Atmos. Res.*, 196, [https://doi.org/10.1016/
626 j.atmosres.2017.06.003](https://doi.org/10.1016/j.atmosres.2017.06.003), 2017c.

627 Liao, H., Yung, Y. L., and Seinfeld, J. H.: Effects of aerosols on tropospheric photolysis
628 rates in clear and cloudy atmospheres, *J. Geophys. Res.*, 104, 23697–23707, 1999.

629 Liao, L., Lou, S. J., Fu, Y., Chang, W. Y., and Liao, H.: Radiative forcing of aerosols
630 and its impact on surface air temperature on the synoptic scale in eastern China [in
631 Chinese], *Chin. J. Atmos. Sci.*, 39, 68–82, doi: 10.3878/j.issn.1006-9895.1402.13302,
632 2015.

633 Lin, Y.-L., Farley, R. D., and Orville, H. D.: Bulk parameterization of the snow field in
634 a cloud model, *J. Clim. Appl. Meteorol.*, 22, 1065–1092, 1983.

635 Lo, J. C.-F., Yang, Z. L., and Pielke Sr, R. A.: Assessment of three dynamical climate
636 downscaling methods using the Weather Research and Forecasting (WRF) model, *J.*
637 *Geophys. Res.*, 113, D09112, doi:10.1029/2007jd009216, 2008.

638 Lohmann, U., and Feichter, J.: Global indirect aerosol effects: A review. *Atmospheric*
639 *Chemistry and Physics*, 5, 715–737, <https://doi.org/10.5194/acp-5-715-2005>, 2005.

640 Lou, S., Liao, H., and Zhu, B.: Impacts of aerosols on surface-layer ozone
641 concentrations in China through heterogeneous reactions and changes in photolysis
642 rates, *Atmos. Environ.*, 85, 123–138, 2014.

643 Otte, T. L.: The impact of nudging in the meteorological model for retrospective air
644 quality simulations. Part I: Evaluation against national observation networks. *J. Appl.*
645 *Meteor. Climatol.*, 47, 1853–1867, 2008.

646 Qin, Y., Li, J., Gong, K., Wu, Z., Chen, M., Qin, M., Huang, L., and Hu, J.: Double

647 high pollution events in the Yangtze River Delta from 2015 to 2019: Characteristics,
648 trends, and meteorological situations, *Sci. Total Environ.*, 792, 148349, 2021.

649 Qiu, Y., Liao, H., Zhang, R., and Hu, J.: Simulated impacts of direct radiative effects
650 of scattering and absorbing aerosols on surface layer aerosol concentrations in China
651 during a heavily polluted event in February 2014, *J. Geophys. Res. Atmos.*, 122,
652 5955–5975, doi:10.1002/2016JD026309, 2017.

653 Qu, Y., Voulgarakis, A., Wang, T., Kasoar, M., Wells, C., Yuan, C., Varma, S., and
654 Mansfield, L.: A study of the effect of aerosols on surface ozone through
655 meteorology feedbacks over China, *Atmos. Chem. Phys.*, 21, 5705–5718,
656 <https://doi.org/10.5194/acp-21-5705-2021>, 2021.

657 Sillman, S.: The relation between ozone, NO_x and hydrocarbons in urban and polluted
658 rural environments, *Atmos. Environ.*, 33, 1821-1845, [https://doi.org/](https://doi.org/10.1016/S1352-2310(98)00345-8)
659 [10.1016/S1352-2310\(98\)00345-8](https://doi.org/10.1016/S1352-2310(98)00345-8), 1999.

660 Skamarock, W., Klemp, J. B., Dudhia, J., Gill, D. O., Barker, D. M., Duda, M., Huang,
661 X. Y., Wang, W., and Powers, J. G.: A description of the advanced research WRF
662 version 3, NCAR technical note NCAR/TN/u2013475, 2008.

663 Tang, G. Q., Zhu, X. W., Xin, J. Y., Hu, B., Song, T., Sun, Y., Zhang, J. Q., Wang, L. L.,
664 Cheng, M. T., Chao, N., Kong, L. B., Li, X., and Wang, Y. S.: Modelling study of
665 boundary-layer ozone over northern China – Part I: Ozone budget in summer, *Atmos.*
666 *Res.*, 187, 128–137, 2017.

667 Tie, X., Geng, F., Li, P., Gao, W., and Zhao, C.: Measurement and modelling of ozone
668 variability in Shanghai, China, *Atmos. Environ.*, 43, 4289–4302, 2009.

669 Wang, W., Li, X., Shao, M., Hu, M., Zeng, L., Wu, Y., and Tan, T.: The impact of
670 aerosols on photolysis frequencies and ozone production in Beijing during the 4-year
671 period 2012–2015, *Atmos. Chem. Phys.*, 19, 9413–9429,
672 <https://doi.org/10.5194/acp19-9413-2019>, 2019.

673 Wild, O., Zhu, X., and Prather, M. J.: Fast-J: Accurate simulation of in- and below-
674 cloud photolysis in tropospheric chemical models, *J. Atmos. Chem.*, 37, 245–282,
675 doi:10.1023/A:1006415919030, 2000.

676 Wu, J., Bei, N., Hu, B., Liu, S., Wang, Y., Shen, Z., Li, X., Liu, L., Wang, R., Liu, Z.,
677 Cao, J., Tie, X., Molina, L. T., Li, G.: Aerosol-photolysis interaction reduces
678 particulate matter during wintertime haze events, *Proc. Natl. Acad. Sci. USA*, 117,
679 9755–9761, 2020.

680 Xing, J., Wang, J. D., Mathur, R., Wang, S. X., Sarwar, G., Pleim, J., Hogrefe, C.,
681 Zhang, Y. Q., Jiang, J. K., Wong, D. and Hao, J. M.: Impacts of aerosol direct effects
682 on tropospheric ozone through changes in atmospheric dynamics and photolysis rates,
683 *Atmos. Chem. Phys.*, 17, 9869–9883, <https://doi.org/10.5194/acp-17-9869-2017>,
684 2017.

685 Zaveri, R. A. and Peters, L. K.: A new lumped structure photochemical mechanism for
686 large-scale applications, *J. Geophys. Res.*, 104, D23, 30387–30415,
687 <https://doi.org/10.1029/1999JD900876>, 1999.

688 Zaveri, R. A., Easter, R. C., Fast, J. D., and Peters, L. K.: Model for simulating aerosol
689 interactions and chemistry (MOSAIC), *J. Geophys. Res.*, 113, D13204,
690 <https://doi.org/10.1029/2007JD008782>, 2008.

691 Zhang, X., Zhang, Q., Hong, C. P., Zheng, Y. X., Geng, G. N., Tong, D., Zhang, Y. X.,
692 and Zhang, X. Y.: Enhancement of PM_{2.5} concentrations by aerosol-meteorology
693 interactions over China. *Journal of Geophysical Research: Atmospheres*, 123, 1179–
694 1194, <https://doi.org/10.1002/2017JD027524>, 2018.

695 Zhang, Y., Wen, X.-Y., and Jang, C. J.: Simulating chemistry–aerosol–cloud–radiation–
696 climate feedbacks over the continental US using the online-coupled Weather
697 Research Forecasting Model with chemistry (WRF/Chem), *Atmos. Environ.*, 44,
698 3568–3582, doi:10.1016/j.atmosenv.2010.05.056, 2010.

699 Zhao, H.; Zheng, Y., and Li, C. Spatiotemporal distribution of PM_{2.5} and O₃ and their
700 interaction during the summer and winter seasons in Beijing, China. *Sustainability*,
701 10, 4519, 2018.

702 Zhu, J., Chen, L., Liao, H., and Dang, R.: Correlations between PM_{2.5} and Ozone over
703 China and Associated Underlying Reasons, *Atmosphere*, 352, 1–15,
704 <https://doi.org/10.3390/atmos10070352>, 2019.

705 Zhu, J., Chen, L., Liao, H., Yang, H., Yang, Y., and Yue, X.: Enhanced PM_{2.5} Decreases
706 and O₃ Increases in China During COVID-19 Lockdown by Aerosol-Radiation
707 Feedback, *Geophys. Res. Lett.*, 48, <https://doi.org/10.1029/2020GL090260>, 2021.

1 **Table 1.** Physical parameterization options used in the simulation.

Options	Schemes
Microphysics scheme	Lin (Purdue) scheme (Lin et al.,1983)
Cumulus scheme	Grell 3D ensemble scheme
Boundary layer scheme	Yonsei University PBL scheme (Hong et al., 2006)
Surface layer scheme	Monin-Obukhov surface scheme (Foken, 2006)
Land-surface scheme	Unified Noah land-surface model (Chen and Dudhia, 2001)
Longwave radiation scheme	RRTMG (Iacono et al., 2008)
Shortwave radiation scheme	RRTMG (Iacono et al., 2008)

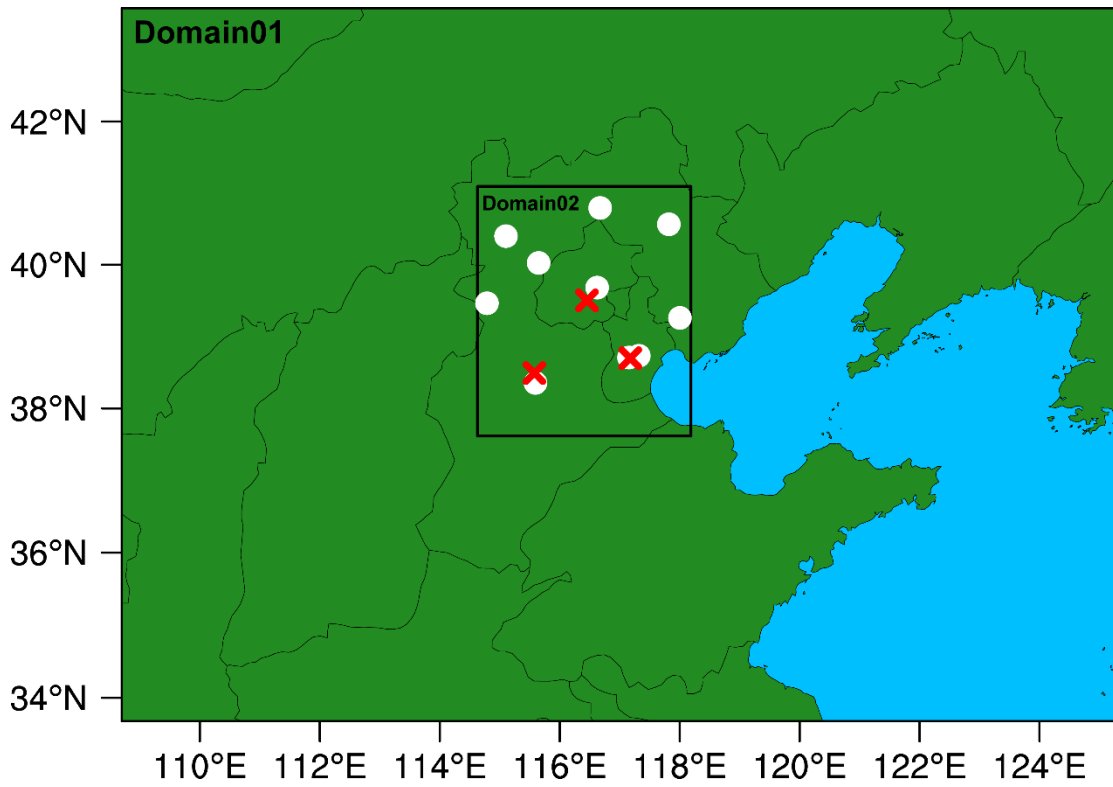
2

1
2
3
4

Table 2. Detailed information of the analyzed episodes, including the impacts of API, ARF and ALL on O₃ concentrations under different air pollution conditions. The numbers in bold indicate the concentrations exceeded the Class II limit of the National Ambient Air Quality Standards of China. The numbers in parentheses indicate the percentage changes in O₃ concentration.

<u>Type</u>	<u>Episode</u>	<u>Time</u>	<u>PM_{2.5} pollution</u> (<u>μg m⁻³</u>)	<u>O₃ pollution</u> (<u>ppb</u>)	<u>API</u> (<u>ppb</u>)	<u>ARF</u> (<u>ppb</u>)	<u>ALL</u> (<u>ppb</u>)
<u>Complex air pollution</u>	<u>Episode1</u>	<u>2014.7.28-2014.8.3</u>	<u>113.3</u>	<u>80.0</u>	<u>-8.5 (-10.2%)</u>	<u>-2.9 (-3.2%)</u>	<u>-11.4 (-13.7%)</u>
	<u>Episode2</u>	<u>2015.7.8-2015.7.13</u>	<u>79.3</u>	<u>89.6</u>	<u>-10.3 (-11.8%)</u>	<u>-1.0 (-1.1%)</u>	<u>-11.3 (-13.0%)</u>
	<u>Episode3</u>	<u>2016.6.5-2016.6.11</u>	<u>76.5</u>	<u>87.6</u>	<u>-9.1 (-11.2%)</u>	<u>-0.9 (-1.0%)</u>	<u>-10.0 (-12.3%)</u>
	<u>Episode4</u>	<u>2017.6.28-2017.7.3</u>	<u>75.4</u>	<u>113.8</u>	<u>-11.4 (-12.2%)</u>	<u>0.7 (0.5%)</u>	<u>-10.7 (-11.6%)</u>
<u>High PM</u>	<u>Episode1</u>	<u>2014.10.7-2014.10.12</u>	<u>223.5</u>	<u>46.9</u>	<u>-15.3 (-29.3%)</u>	<u>-3.9 (-6.2%)</u>	<u>-19.2 (-37.6%)</u>
	<u>Episode2</u>	<u>2014.4.7-2014.4.11</u>	<u>111.7</u>	<u>54.8</u>	<u>-7.3 (-16.9%)</u>	<u>-2.4 (-4.7%)</u>	<u>-9.7 (-22.6%)</u>
<u>High O₃</u>	<u>Episode1</u>	<u>2017.6.15-2017.6.21</u>	<u>61.9</u>	<u>103.6</u>	<u>-4.5 (-5.3%)</u>	<u>-0.1 (-0.1%)</u>	<u>-4.6 (-5.5%)</u>
	<u>Episode2</u>	<u>2017.7.12-2017.7.17</u>	<u>45.6</u>	<u>100.4</u>	<u>-3.8 (-4.5%)</u>	<u>-0.1 (-0.1%)</u>	<u>-3.9 (-4.6%)</u>
<u>Low POL</u>	<u>Episode1</u>	<u>2016.6.13-2016.6.18</u>	<u>36.5</u>	<u>62.4</u>	<u>-4.4 (-6.8%)</u>	<u>-0.6 (-1.0%)</u>	<u>-5.0 (-7.9%)</u>
	<u>Episode2</u>	<u>2016.7.13-2016.7.17</u>	<u>38.3</u>	<u>55.9</u>	<u>-1.9 (-2.9%)</u>	<u>-0.5 (-0.7%)</u>	<u>-2.4 (-3.7%)</u>

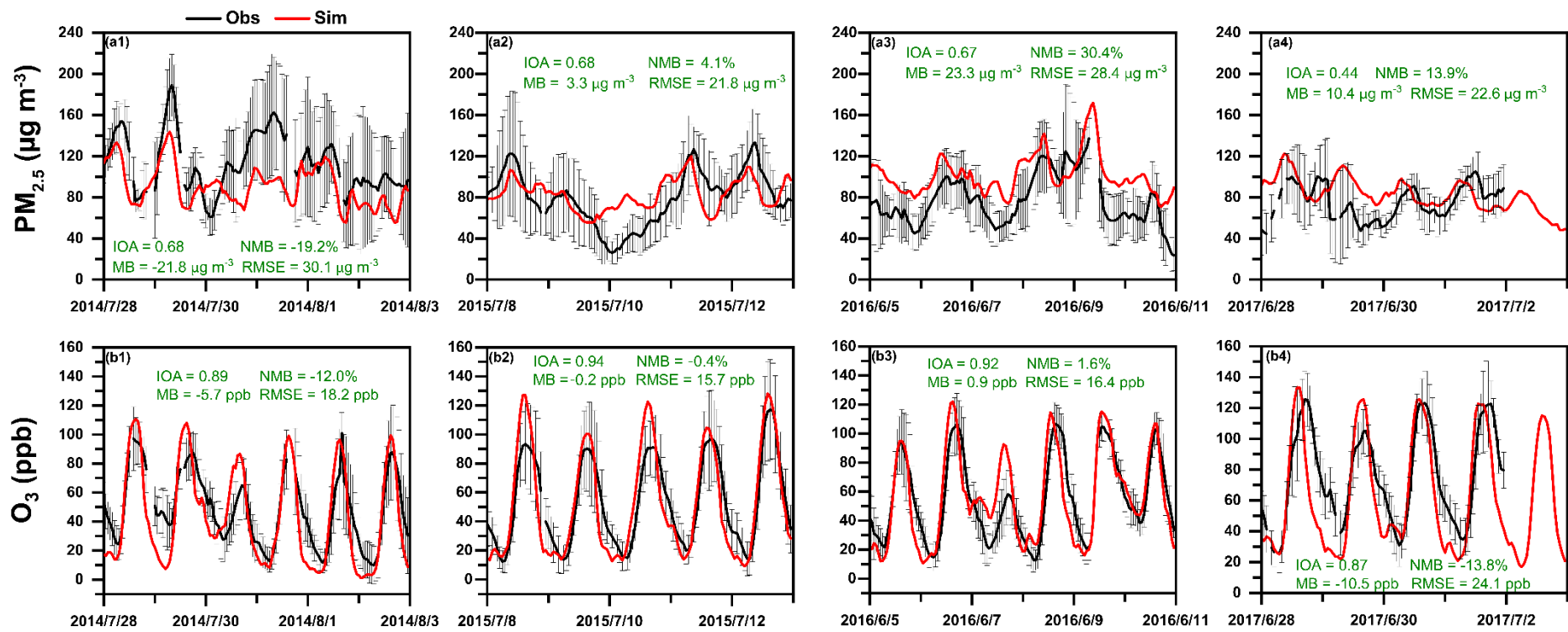
5



1

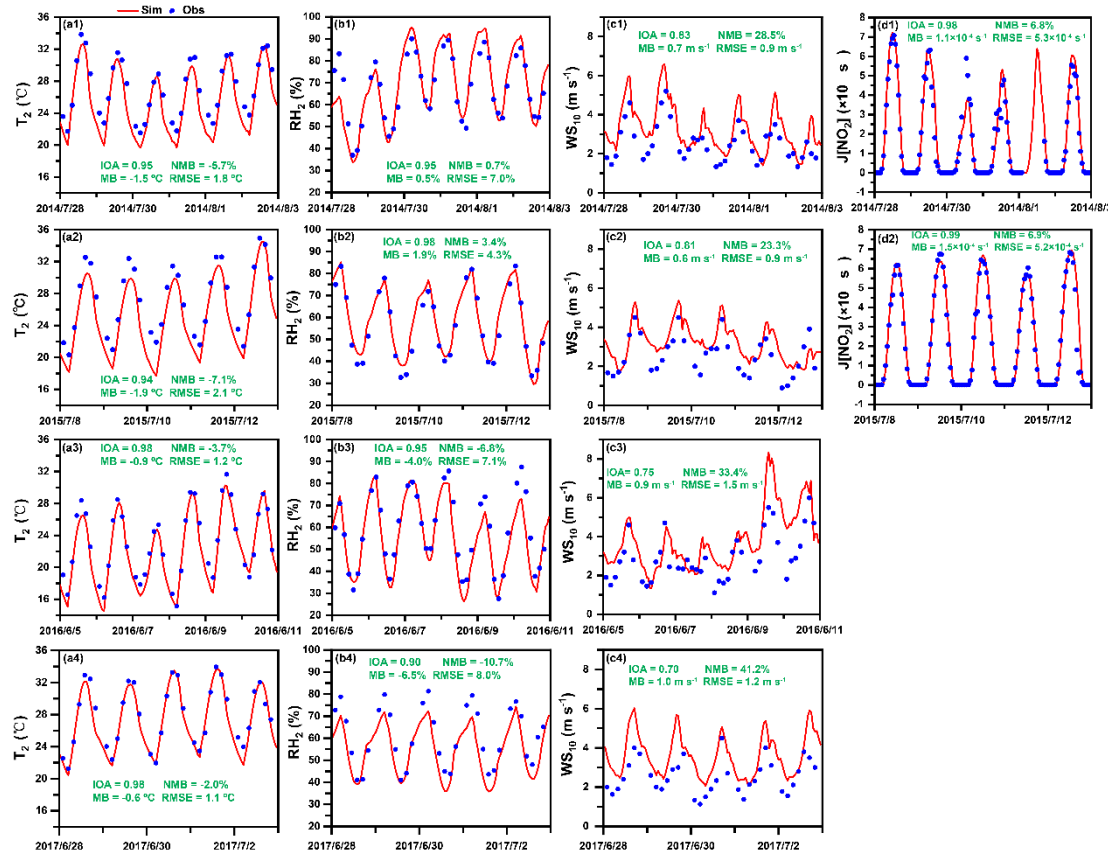
2 **Figure 1.** Map of the two WRF-Chem modeling domains with the locations of
 3 meteorological (white dots) and environmental (red crosses) observation sites used for
 4 model evaluation.

5



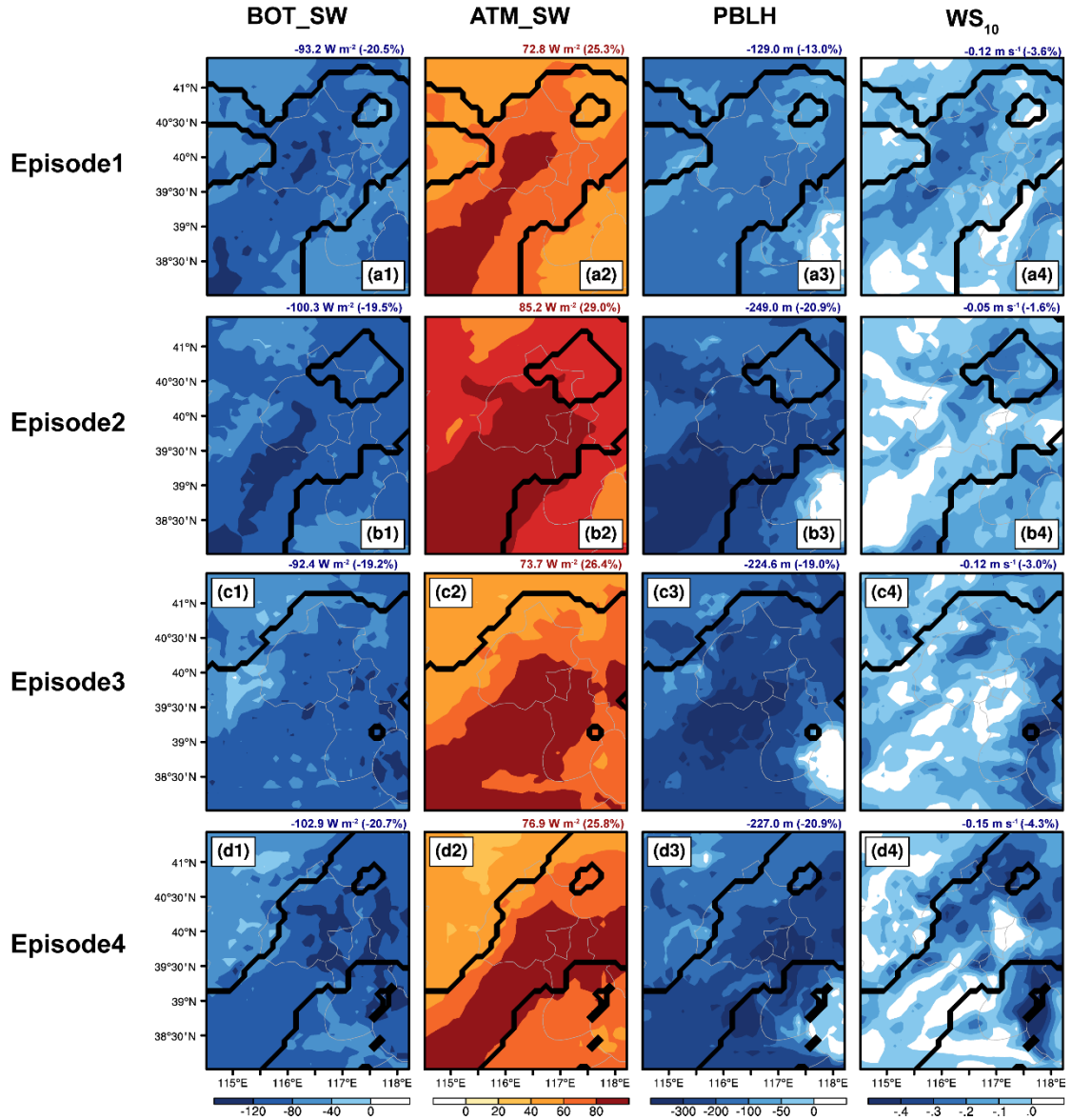
1
2
3
4
5
6

Figure 2. Time series of observed (black) and simulated (red) hourly surface (a) $PM_{2.5}$ and (b) O_3 concentrations averaged over the thirty-two observation sites in Beijing, Tianjin, and Baoding during 28 July to 3 August 2014 (Episode1, a1-b1), 8-13 July 2015 (Episode2, a2-b2), 5-11 June 2016 (Episode3, a3-b3) and 28 June to 3 July 2017 (Episode4, a4-b4). The error bars represent the standard deviations. The calculated index of agreement (IOA), mean bias (MB), normalized mean bias (NMB) and root-mean-square error (RMSE) are also shown.



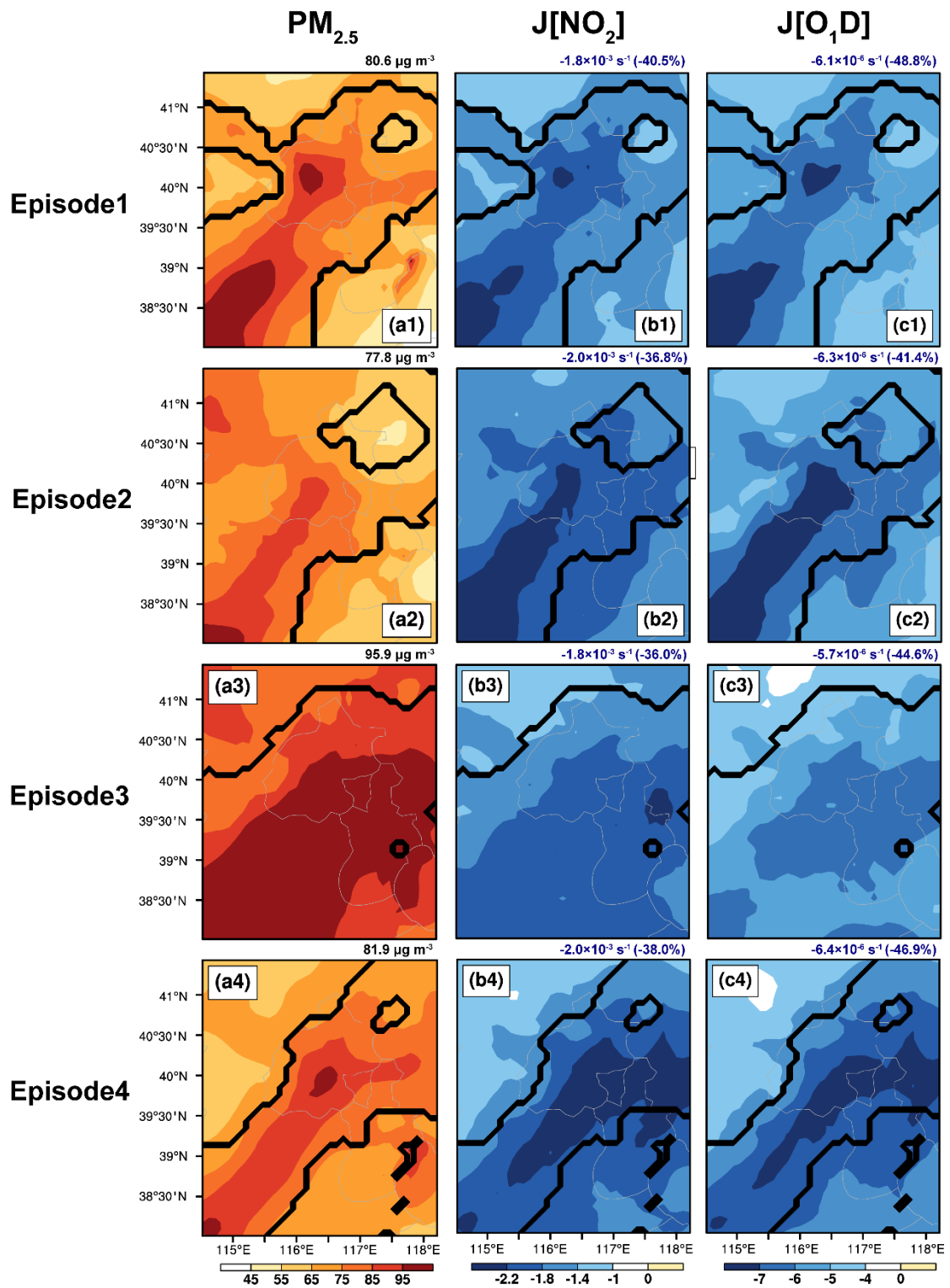
1

2 **Figure 3.** Time series of 3-hourly observed (blue dots) and hourly simulated (red lines) (a) 2-m temperature (T_2), (b) 2-m relative humidity (RH_2),
 3 (c) wind speed at 10 m (WS_{10}) averaged over ten meteorological observation stations, and (d) surface photolysis rate of NO_2 ($J[NO_2]$) during 28
 4 July to 3 August 2014 (Episode1, a1-d1), 8-13 July 2015 (Episode2, a2-d2), 5-11 June 2016 (Episode3, a3-c3) and 28 June to 3 July 2017 (Episode4,
 5 a4-c4). The calculated index of agreement (IOA), mean bias (MB), normalized mean bias (NMB) and root-mean-square error (RMSE) are also
 6 shown.



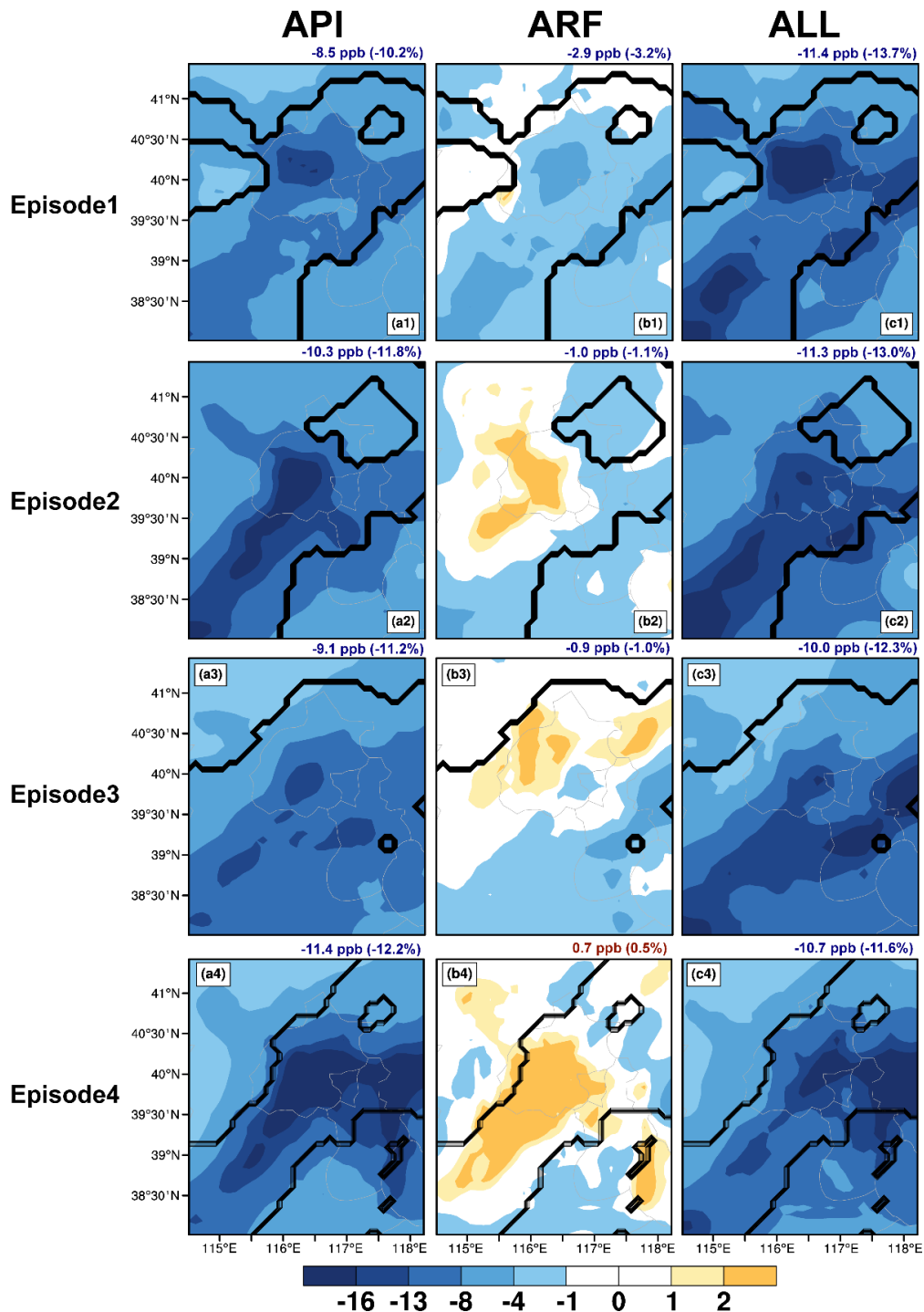
1

2 **Figure 4.** The impacts of aerosol-radiation interactions on shortwave radiation at the
3 surface (BOT_SW), shortwave radiation in the atmosphere (ATM_SW), PBL height
4 (PBLH), and 10-m wind speed (WS₁₀) in the daytime (08:00-17:00 LST) during 28 July
5 to 3 August 2014 (Episode1), 8-13 July 2015 (Episode2), 5-11 June 2016 (Episode3)
6 and 28 June to 3 July 2017 (Episode4). The regions sandwiched between two black
7 lines are defined as the complex air pollution areas (CAPAs) where the mean daily
8 PM_{2.5} and MDA8 O₃ concentrations in BASE case are larger than 75 μg m⁻³ and 80 ppb.
9 The calculated changes (percentage changes) averaged over CAPAs are also shown at
10 the top of each panel.



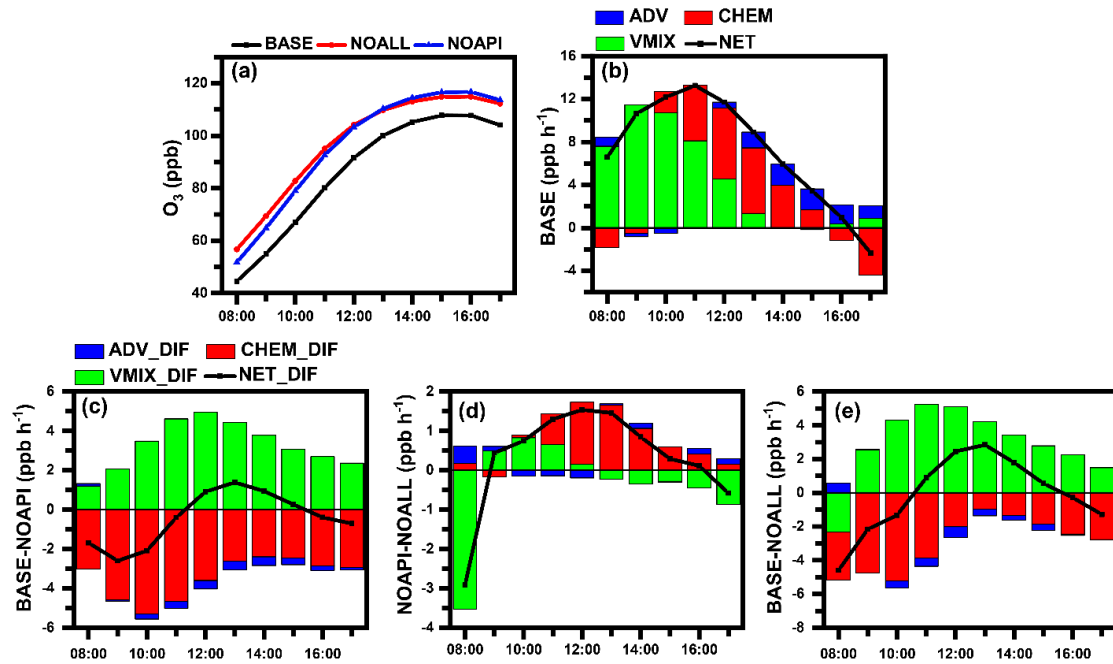
1

2 **Figure 5.** Spatial distributions of (a) simulated surface-layer $PM_{2.5}$ concentrations in
 3 BASE cases, and the changes in surface (b) $J[NO_2]$ and (c) $J[O^1D]$ due to aerosol-
 4 radiation interactions in the daytime (08:00-17:00 LST) during 28 July to 3 August
 5 2014 (Episode1), 8-13 July 2015 (Episode2), 5-11 June 2016 (Episode3) and 28 June
 6 to 3 July 2017 (Episode4). The calculated values (percentage changes) averaged over
 7 CAPAs are also shown at the top of each panel.



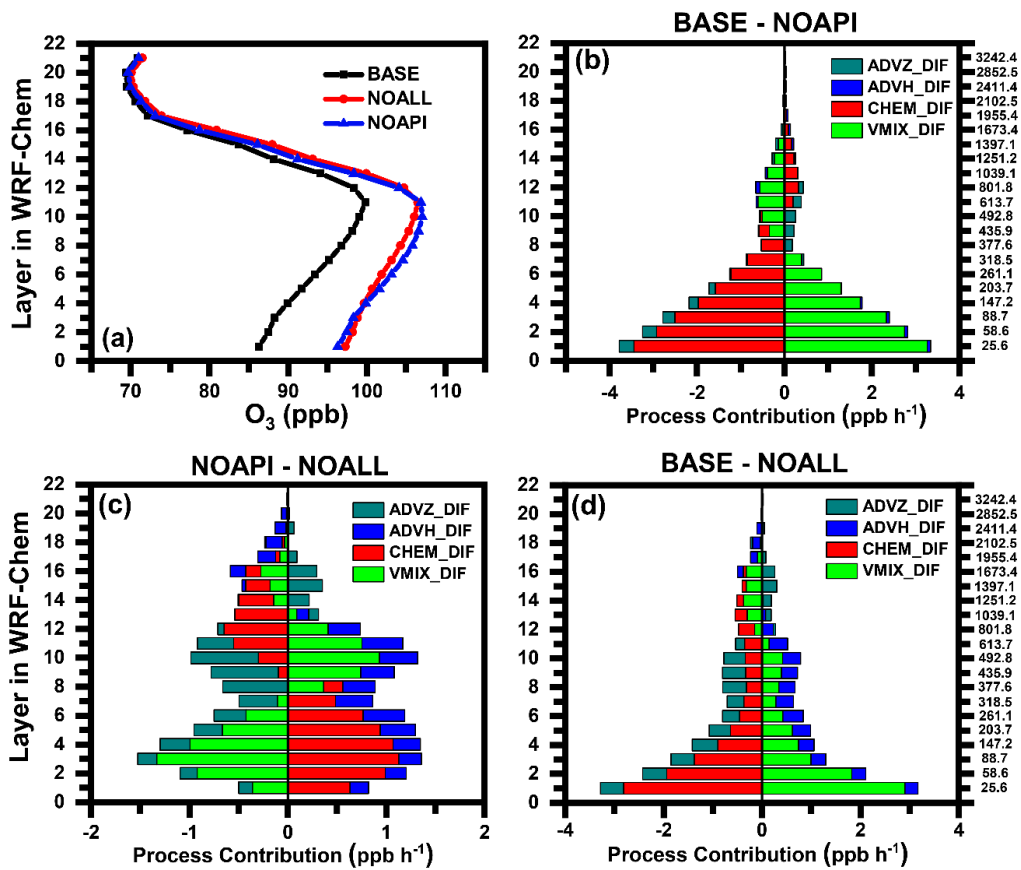
1
2
3
4
5
6
7
8
9

Figure 6. The changes in surface-layer ozone due to (a) aerosol-photolysis interaction (API), (b) aerosol-radiation feedback (ARF), and (c) the combined effects (ALL, defined as API+ARF) in the daytime (08:00-17:00 LST) during 28 July to 3 August 2014 (Episode1), 8-13 July 2015 (Episode2), 5-11 June 2016 (Episode3) and 28 June to 3 July 2017 (Episode4). The changes (percentage changes) in O₃ concentrations caused by API, ARF and ALL averaged over CAPAs are also shown at the top of each panel.



1
2
3
4
5
6
7
8
9
10
11
12

Figure 7. Temporal evolution characteristics of aerosol-radiation interactions on O₃ averaged over the four episodes. (a) Diurnal variations of simulated surface O₃ concentrations in BASE (black dotted line), NOAPI (blue dotted line), and NOALL (red dotted line) cases over CAPAs. (b) The hourly surface O₃ changes induced by each physical/chemical process using the IPR analysis method in BASE case. (c-e) Changes in hourly surface O₃ process contributions caused by API (BASE minus NOAPI), ARF (NOAPI minus NOALL), and ALL (BASE minus NOALL) over CAPAs during the daytime (08:00-17:00 LST). The black lines with squares denote the net contribution of all processes (NET, defined as VMIX+CHEM+ADV). Differences of each process contribution are denoted as VMIX_DIF, CHEM_DIF, ADV_DIF, and NET_DIF.



1

2 **Figure 8.** The impacts of aerosol-radiation interactions on vertical O₃ averaged over
 3 the four episodes. (a) Vertical profiles of simulated O₃ concentrations in BASE (black
 4 dotted line), NOAPI (blue dotted line), and NOALL (red dotted line) cases over CAPAs.
 5 (b-d) Changes in O₃ budget due to API, ARF, and ALL over CAPAs during the daytime
 6 (08:00-17:00 LST). Differences of each process contribution are denoted by
 7 ADVZ_DIF, ADVH_DIF, CHEM_DIF, and VMIX_DIF.

8

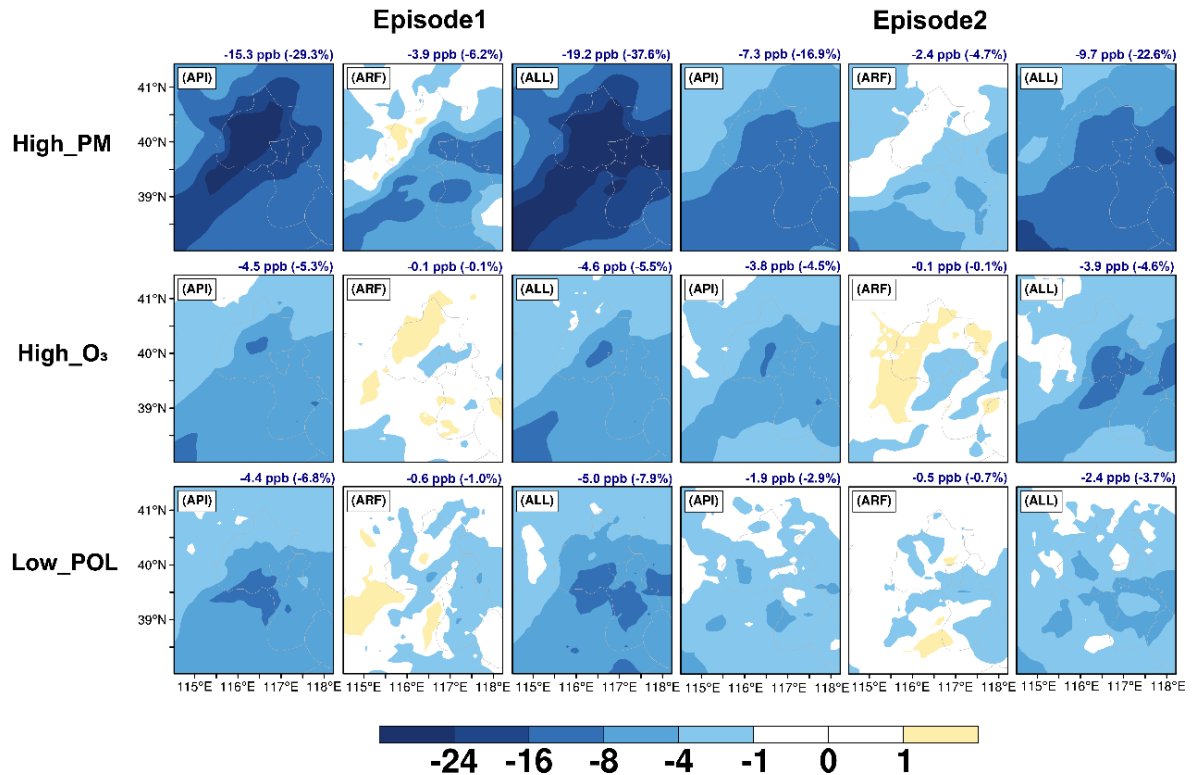


Figure 9. The changes in surface-layer O₃ due to aerosol-photolysis interaction (API), aerosol-radiation feedback (ARF), and the combined effects (ALL, API+ARF) in the daytime (08:00-17:00 LST) of 7-12 October 2014 (High PM_Episode1), 7-11 April 2014 (High PM_Episode2), 15-21 June 2017 (High O₃_Episode1), 12-17 July 2017 (High O₃_Episode2), 13-18 June 2016 (Low POL_Episode1), and 13-17 July 2016 (Low POL_Episode2). The changes (percentage changes) in O₃ concentrations caused by API, ARF and ALL averaged over the entire simulated domain are also shown at the top of each panel.